Defense Threat Reduction Agency
8725 John J. Kingman Road, MS 6201
Fort Belvoir, VA 22060-6201

DTRA-TR-03-18

TECHNICAL REPORT

Surface Wave Detection and Measurement Using a One Degree Global Dispersion Grid

May 2006

DSWA01-98-C-0154

Jeffry L. Stevens, et al.

Prepared by:
Science Applications International Corporation
10260 Campus Point Drive
San Diego, CA 92121

DARE Tracking
73741

DESTRUCTION NOTICE

FOR CLASSIFIED documents, follow the procedures in DoD 5550.22-M, National Industrial Security Program Operating Manual, Chapter 5, Section 7 (NISPOM) or DoD 5200.1-R, Information Security Program Regulation, Chapter 1X.

FOR UNCLASSIFIED limited documents, destroyed by any method that will prevent disclosure of contents or reconstruction of the document.

Retention of this document by DoD contractors is authorized in accordance with DoD 5220.22M, Industrial Security manual.

PLEASE NOTIFY THE DEFENSE THREAT REDUCTION AGENCY, ATTN: IMMI, 8725 JOHN J. KINGMAN ROAD, MS-6201, FT. BELVOIR, VA 22060-6201. IF YOUR ADDRESS IS INCORRECT, IF YOU WISH IT DELETED FROM THE DISTRIBUTION LIST, OR IF THE ADDRESSEE IS NO LONGER EMPLOYED BY YOUR ORGANIZATION.

DISTRIBUTION LIST UPDATE

This mailer is provided to enable DTRA to maintain current distribution lists for reports. (We would appreciate you providing the requested information.)

- ❑ Add the individual listed to your distribution list.
- ❑ Delete the cited organization/individual.
- ❑ Change of address.

Note:
Please return the mailing label from the document so that any additions, changes, corrections or deletions can be made easily. For distribution cancellation or more information call DTRA/BDLMI (703) 767-4725.

NAME: _____

ORGANIZATION: _____

OLD ADDRESS	NEW ADDRESS
_____	_____
_____	_____
_____	_____

TELEPHONE NUMBER: ( ) _____

DTRA PUBLICATION NUMBER/TITLE	CHANGES/DELETIONS/ADDITONS, etc. *(Attach Sheet if more Space is Required)*
_____	_____
_____	_____
_____	_____

DTRA or other GOVERNMENT CONTRACT NUMBER: _____

CERTIFICATION of NEED-TO-KNOW BY GOVERNMENT SPONSOR (if other than DTRA):

SPONSORING ORGANIZATION: _____

CONTRACTING OFFICER or REPRESENTATIVE: _____

SIGNATURE: _____

DEFENSE THREAT REDUCTION AGENCY
ATTN: BDLMI
8725 John J Kingman Road, MS 6201
Fort Belvoir, VA 22060-6201

DEFENSE THREAT REDUCTION AGENCY
ATTN: BDLMI
8725 John J Kingman Road, MS 6201
Fort Belvoir, VA 22060-6201

REPORT DOCUMENTATION PAGE

Form Approved
OMB No. 0704-0188

1. REPORT DATE *(DD-MM-YYY)*	2. REPORT TYPE	3. DATES COVERED *(From - To)*
April 2006	Technical Report	

4. TITLE AND SUBTITL
Surface Wave Detection and Measurement Using a One Degree Global Dispersion Grid

5a. CONTRACT NUMBER
DSWA 01-98-C-0154

5b. GRANT NUMBER

5c. PROGRAM ELEMENT NUMBER
4613

6. AUTHOR(S)
Jeffry L. Stevens, et al.

5d. PROJECT NUMBER
CD

5e. TASK NUMBER
CD

5f. WORK UNIT NUMBER
DH66450

7. PERFORMING ORGANIZATION NAME(S) AND ADDRESS(ES)

Science Applications International Corporation
10260 Campus Point Drive
San Diego, CA 92121-1578

8. PERFORMING ORGANIZATION REPORT NUMBER

9. SPONSORING / MONITORING AGENCY NAME(S) AND ADDRESS(ES)
Defense Threat Reduction Agency
8725 John J. Kingman Rd., MS 6201
Fort Belvoir, VA 22060-6201

10. SPONSOR/MONITOR'S ACRONYM(S)
DTRA

11. SPONSOR/MONITOR'S REPORT NOS.
TR-03-18

12. DISTRIBUTION / AVAILABILITY STATEMENT
Approved for public release; distribution is unlimited.

13. SUPPLEMENTARY NOTES

14. ABSTRACT

We develop high resolution earth and dispersion models for use in detection and measurement of surface waves. The models consist of approximately 550 distinct crust and upper mantle structures, with surface layering and/or ocean depths that vary on a one-degree grid to create a total of 64,800 earth models. Tomographic conversion is performed for the crust and upper mantle models using a data set of approximately 540,000 phase and group velocity dispersion measurements. The starting models for the inversion are a modification of Crust 2.0 over AK135. Surface sediments are defined using the global sediment maps of Laske and Masters and ocean bathymetry is defined using Etopo5. We have implemented a new procedure for surface wave identification, in which data is phase-match filtered, then narrow-band filters are applied to the compressed waveform. Detections using the one-degree model with phase-matched filtering increased by 40% compared to the five-degree model currently in use at the IDC without phase-matched filtering. We use long-period waveforms from nuclear explosions to assess the location capability of automated Rayleigh wave travel-time packs. Good locations can be determined with surface waves provided that the paths are relatively short and an accurate dispersion model is available.

15. SUBJECT TERMS
Surface wave, Dispersion curve, Phase-matched filter, Moment, Location, Regionalization

a. REPORT	b. ABSTRACT	c. THIS PAGE	17. LIMITATION OF ABSTRACT	18. NUMBER OF PAGES	19a. NAME OF RESPONSIBLE PERSON
Unclassified	Unclassified	Unclassified	SAR	41	19b. TELEPHONE NUMBER *(include area code)*

CLASSIFIED BY:

N/A since Unclassified

DECLASSIFIED BY:

N/A since Unclassified

Table of Contents

Section			Page
	List of Figures		iv
	List of Tables		vi
	Acknowledgement		vii
1	Introduction and Summary		1
2	Improved Dispersion Models		2
	2.1	Overview	2
	2.2	Data	3
	2.3	Tomographic Inversion	3
	2.4	Inversion on a Five Degree Grid	5
	2.5	Methods for Refining Inversions	5
		2.5.1 Finding new model types	5
		2.5.2 Selection of new model types from resolution calculations	6
	2.6	Five Degree Models	7
	2.7	Inversion on a One Degree Grid	9
	2.8	One Degree Models	10
3	New Detection Algorithm Using Phase-Matched Filtering		13
4	Tests of Dispersion Models		15
	4.1	IMS Data	15
	4.2	Nuclear Explosion Data	16
5	Use of Surface Waves to Improve Location		20
6	Definition of M_s and Path Corrected Spectral Magnitudes		23
	6.1	Spectral Magnitudes and Scalar Moment	24
	6.2	Regionalization	26
7	Depth Discrimination Using Surface Wave Spectra		27
8	Conclusion and Recommendations		29
9	References		30
Appendix			
A	Data Deliverable		A-1

List of Figures

Figure		Page
1	Map of the diagonal elements of the resolution matrix for group velocity measurements in the frequency range 0.025 to 0.0330 Hz using an approximation of the SVD using the Lanczos method and 573 out of a possible 2592 singular values	2
2	50-second phase velocity	7
3	50-second group velocity	7
4	20-second phase velocity	8
5	20-second group velocity	8
6	50-second period phase velocity map	10
7	50-second period group velocity map	11
8	20-second period phase velocity map	11
9	20-second period group velocity map	12
10	Shear wave velocity depth profiles for the main 15 ocean types	12
11	Data in the 5 km/sec to 2 km/sec time window from an m_b 3.9 South Pacific earthquake after transformation to a KS36000 instrument and after compression by phase-matched filtering	13
12	The narrow-band filter detection test compares measured group velocity with a regionalized group velocity model	14
13	Improvement in the number of detections for a day of data with improvements in the model and with phase-matched filtering	15
14	Surface waves recorded at MAJO from 5 NTS explosions bandpass filtered near 20 seconds	17
15	The great circle path from NTS to MAJO is a grazing path along the northern boundary of the Pacific Ocean	18
16	Histogram of measured group velocities of 20-second Rayleigh waves from explosions at all major test sites	21

List of Figures (continued)

Figure		Page
17	Mean and two standard deviation error bounds of distance estimates from single stations for different frequencies	21
18	Location errors for Semipalatinsk explosions	22
19	M_s:m_b plot for a data set of earthquakes recorded at the PIDC and historical explosions	23
20	Log M_0:m_b plot for a data set of earthquakes recorded at the PIDC and historical explosions	26
21	Scalar moment estimate for an explosion and earthquake calculated for several earthquake depths	27
22	Observed path corrected spectral magnitudes for events with a range of depths for day 2000333	28

List of Tables

Table		Page
1	Summary of the new Earth parameterization	10
2	40-second group velocity % average residuals	16
3	20-second group velocity % average residuals	16
4	Location errors for 3 methods and the number of stations used for each	20

Acknowledgements

We would like to thank Mike Ritzwoller, Anatoli Levshin and Antonio Villasenor of the University of Colorado, Brian Mitchell and Bob Herrmann of St. Louis University, Goran Ekstrom of Harvard University, Andrew Curtis of Utrecht University, Mike Pasyanos and Bill Walter of Lawrence Livermore National Laboratories, and their coworkers for the use of their data and models in this project. We thank David Harkrider and Nazieh Yacoub for useful and informative discussions.

Section 1
Introduction and Summary

The primary goal of this project is to improve the capability to identify and measure surface waves for the purpose of earthquake/explosion discrimination. We develop improved, higher resolution earth and dispersion models. The models consist of approximately 550 distinct crust and upper mantle structures, with surface layering and/or ocean depths that vary on a one degree grid. There are a total of 64,800 earth models and dispersion curves, but the tomographic inversion is performed only for the 550 distinct crust and upper mantle models, with the shallow structure constrained by other information. The data set used in the inversion now consists of approximately 540,000 phase and group velocity dispersion measurements obtained from a variety of sources. The starting models for the inversion are a modification of Crust 2.0 (Laske et al., 2001; Bassin et al., 2000) over AK135 (Kennett et al., 1995). Surface sediments are defined using the global sediment maps of Laske and Masters (1997), and ocean bathymetry is defined using the Etopo5 topographic data set.

Automatic identification of surface waves at the International Data Centre is currently performed by narrow-band filtering the data at several frequencies, and then comparing the arrival times with a regionalized dispersion model. We have implemented and tested a new procedure in which we first phase-match filter the data and then apply narrow-band filters to the compressed waveform and use a detection test similar to the current test. This allows us to take advantage of the improved signal-to-noise ratio of the phase-match filtered waveforms, while retaining the robustness of narrow-band filtering for frequency-dependent signal identification. After phase-matched filtering, the predicted arrival time is zero at all frequencies, so we test to see if the arrivals are within a time window similar to that used in the existing test. To test the procedure, we processed the same data set using five degree and one degree models with and without phase-matched filtering. Detections using the one degree model with phase-matched filtering increased by 40% compared to the five degree model currently in use at the IDC without phase-matched filtering.

We use long-period waveforms from historic nuclear explosions to assess the potential of automated Rayleigh wave travel-time picks to improve seismic event locations. The improved accuracy of locations reported by Yacoub (2000), based on 20-second Rayleigh waves, provided the impetus for this work. Although surface wave arrival times cannot be measured as accurately as body wave arrivals, that surface waves are much slower means that accurate locations can be achieved. We find that good locations can be determined with surface waves, which could potentially improve locations made with body waves alone provided that the paths are relatively short and an accurate dispersion model is available for the region. This may be especially important for small events with few total measurements. To assess the value of single surface wave measurements for that purpose, we also estimate the accuracy of single-station distance estimates.

Section 2
Improved Dispersion Models

2.1 Overview

The most important information required for improving surface wave detection and measurement is accurate global dispersion maps. Consequently, this research program has concentrated on the development of three-dimensional velocity models of the earth's crust and upper mantle by tomographic inversion of surface wave dispersion measurements. This work uses an extension of the technique described by Stevens and McLaughlin (2001), in which a global earth model with 149 distinct model types on a five degree grid was developed. That model is now being used for routine surface wave identification at the International Data Centre (IDC). The technique used at the IDC is to compare predicted group velocity dispersion curves derived from these regionalized models with measured dispersion curves from observed surface waves. As discussed later, phase velocities derived from these earth models can also be used to develop phase-matched filters to improve signal to noise ratio and optimize the detection test.

Development of improved earth models and dispersion curves has proceeded using the following approach:

1. The starting point was the 5 degree IDC 149 model set (Stevens and McLaughlin, 2001) which was based on approximately 90,000 dispersion measurements.
2. New dispersion measurements were added to the data set and the same model set was reinverted with the new data.
3. New model types were added in areas with increased data or where the data misfit indicated that new model types were required and a new inversion was performed with the larger data and model set.
4. A procedure was developed for including shallow structure, particularly sediment thicknesses and ocean depths, on a one degree grid while inverting for a limited set of distinct models, most of which remained on a five degree grid, in the crust and upper mantle.
5. The locations and boundaries of the underlying model types were redefined, starting with the Crust 2.0 model, so that they follow plate boundaries and other geologic constraints. The inversion technique was also modified to allow small variations in Moho depth and layer thickness to be defined on a one degree grid for each model type.

With our current approach, the inversion is performed for shear velocity structures in approximately 550 distinct crust and upper mantle model types, but the shallow structure, bathymetry, as well as small changes in layer thickness and Moho depth, can vary on a one degree grid (64,800 distinct models). Below the maximum inversion depth (~300 km) the Earth model is fixed to match AK 135. The top few km of the model (consisting of water, ice and/or sediments) is fixed and matches data from 1 degree bathymetry maps and 1 degree sediment maps. One advantage of inverting for a fixed set of crust and upper mantle structures is that it reduces the problem to a more manageable size. An earth model consisting of 16200 2 by 2

degree cells and with 12 layers per cell would have 200,000 free parameters. Our current model consists of 556 model types, which reduces the total number of free parameters to 8400. Other advantages of this type of inversion are that it uses all frequencies (and both phase and group velocity) at once, with different frequencies resolving different length scales; the technique keeps similar structures consistent with each other, preventing the fluctuations in nearby frequency points common in more traditional group velocity inversions; and it allows Moho depths, subcrustal layer thicknesses, and lateral boundaries between geologic regions to be added to the model as fixed a priori information. The principal disadvantages are that distinct model types must be chosen carefully and added sparingly if needed, and that there is no smoothness constraint between adjacent structures. The tradeoff here is that without an explicit continuity condition we can incorporate real discontinuities such as ocean/continent boundaries and boundaries between tectonic regions, but the inversions will in some cases produce adjacent models with anomalous lateral discontinuities.

2.2 Data

The data used to derive our earth models consist of more than 540,000 measurements of surface wave group and phase velocity dispersion from earthquakes and explosions. These measurements were obtained from various sources and are for frequencies ranging between 0.005 and 0.1667 Hz with the great majority of observations between 0.01 and 0.1 Hz. The data set has been derived from a variety of regional and global studies including the following: global surface wave group velocities from earthquakes derived using PIDC GSETT3 data (Stevens and McLaughlin, 1996), augmented with more recent measurements derived from PIDC data; surface wave phase and group velocity dispersion curves from underground nuclear test sites (Stevens, 1986; Stevens and McLaughlin, 1988), calculated from earth models for 270 paths (test site – station combinations) at 10 frequencies between 0.015 and 0.06 Hz; phase and group velocity measurements for western Asia and Saudi Arabia from Mitchell et al.(1996) for 12 paths at 17 frequencies between 0.012 and 0.14 Hz; the global phase velocity model of Ekstrom et al. (1996) for 9 periods between 35 and 150 seconds calculated for each 5 degree grid block from a spherical harmonic expansion of order $l = 40$; group velocity measurements for Eurasia from Ritzwoller et al.(1996) and Levshin et al.(1996) for 20 frequencies between 0.004 and 0.1 Hz with 500 to 5000 paths per frequency; Antarctic and South American group velocity measurements from the University of Colorado (Vdovin et al., 1999; Ritzwoller et al., 1999); high frequency Eurasian dispersion measurements from University of Colorado (Levshin and Ritzwoller, pers. comm., 2001), and a large set of dispersion measurements from Saudi Arabia provided by Herrmann and Mokhtar at St. Louis University.

2.3 Tomographic Inversion

Certain types of structures can significantly affect surface wave dispersion, but either cannot be resolved adequately by the data, or require a grid finer than five degrees for resolution. It is best to constrain these structural features using independent data. The effects come from variations in sediments and in water depths, and the approximation, by fixed size cells, of boundaries between zones, for example plate boundaries and coastlines. Important information is lost when sediment thicknesses and properties, and depth of water columns are averaged over all of the cells comprising a particular model type. We therefore developed a method for incorporating

sediments, bathymetry, coastlines and zone boundaries determined on a 1 degree grid into our inversions while retaining a relatively small number of distinct crust and upper mantle models.

Each equation in the tomographic system is of the form shown below. S_g is the slowness of the g^{th} 1 degree cell; m_j is the shear wave velocity of the j^{th} layer where j spans all the adjustable layers of all model types. X_{ig} is the length of i^{th} raypath traveled in the g^{th} cell, ΔT_i is the travel time residual for the i^{th} raypath, and X_i is the total length of the i^{th} raypath.

$$\frac{1}{X_i}\sum_j \Delta m_j \sum_g \frac{\partial S_g}{\partial m_j} X_{ig} = \frac{\Delta T_i}{X_i} \tag{1}$$

Some of the inversion data set consists of model interpretations, such as the Harvard phase velocity models. For these cases we have a dispersion value at each point rather than a path averaged value, so equation 1 becomes:

$$\sum_j \Delta m_j \frac{\partial S_g}{\partial m_j} = \Delta S_g \tag{2}$$

where ΔS_g is the slowness residual.

The tomographic inversion has the form shown in equations 1 and 2. These are combined into a single matrix equation $\mathbf{A}\Delta\mathbf{m} = \mathbf{S}$ where there is one column of matrix **A** for each model layer, and one row for each data point. Predicted dispersion and partial derivatives of the model are calculated from 64,800 one degree cells which carry the information about sediments and bathymetry as well as crust and upper mantle structure. The free parameters, however, indexed with j, span a coarser scale, that of the model types. These equations, plus equations for damping and smoothing, are solved using the LSQR method (Nolet, 1987). The damping and smoothing equations each have dimension equal to the number of model layers and are appended to the equations above.

Regularization is controlled by two parameters, one for a vertical smoothing condition applied to layers in each model type, and a damping parameter. These have been applied in two different forms. In the earlier 5 degree inversions, a smoothing constraint was applied that minimized the difference in smoothness between the starting model and the final model, and the damping constraint minimized the difference between the shear velocity values of the starting and final models for each iteration. More recent inversions have adopted a different approach. The inversions now apply a smoothness condition to the model, but allow discontinuities at the Moho and at the sediment/crustal or ocean/crustal boundaries. Damping now uses the initial starting model derived as described above as a constraint on the inversion, rather than the starting model that changes between iterations. The effect of this is to stabilize the inversion while finding a solution that matches the data as well as possible, consistent with geophysical constraints and a model that is vertically smooth between known discontinuities.

2.4 Inversion on a Five Degree Grid

We briefly discuss the five degree models that were developed in the earlier phases of this project. The five degree models consist of 2592 5x5 degree cells, each one associated with a particular model type. Each model type consists of plane layers, each with uniform P and S wave velocities, density and Q, with layers extending to a depth of about 220 km. As with the one degree models, the S-wave velocities are treated as free parameters which are estimated by tomographic inversion of observations of group and phase velocity dispersion. The surface wave dispersion observations are a large subset of those used for the one degree inversions.

Stevens and McLaughlin (2001) describe development of a global earth model with 149 distinct models on a five degree grid that is now used for surface wave identification at the PIDC and IDC. The development used global tomographic inversion of about 90,000 dispersion measurements, using the Crust 5.1 model (Mooney, et al., 1998) as a starting point. This process was continued by Stevens and Adams (1999, 2000) who increased the number of data points to more than 248,000 and increased the number of earth model types to 399.

2.5 Methods for Refining Inversions

The number of free parameters in the global model can be increased as the number of data points is increased. In this section, we describe procedures for finding new model types, and give an example showing how these procedures were applied for one of the five degree inversions.

2.5.1 Finding new model types.

Addition of new data permits us to increase the number of model types and therefore the total number of free parameters. To select new model types we use the results of 2D group velocity tomography to identify cells with the largest apparent differences between observed and calculated dispersion (Stevens and Adams, 1999). "2D tomography" refers to the more traditional type of tomographic inversion in which we invert observed group velocity dispersion measurements over a narrow frequency band to find the group velocities for each cell. For each of 9 frequency bands we perform a tomographic inversion using the group velocity residuals from the 3D tomographic inversion (inversion for earth structure using both phase and group velocity at all frequencies) as data, and perturbations in the group velocities for each of the 2592 cells as parameters. Cells with large perturbations for several frequency bands are selected as possible candidates for association with new model types. This is done because spurious fluctuations may occur between frequencies in the 2D inversions, but a consistent trend between frequencies is a good indicator of a real physical effect. In addition, spurious perturbations can occur in areas of poor resolution, usually caused by the effect of a small number of inaccurate measurements. Therefore, as an additional guide, we compute resolution matrices of the 2D tomographic systems of equations. Well-resolved cells with large group velocity perturbations are given new model types and poorly resolved cells with large perturbations are not unless there is other supporting evidence. We use the Lanczos method of approximating SVDs for sparse matrices described and applied to tomography problems by Vasco *et al.* (1999), and code written by Berry (1992).

Figure 1 shows the diagonal elements of an approximation of the resolution matrix for the 2D tomographic system using group velocity measurements for frequencies above and including 0.025 Hz and below 0.0330 Hz. This approximation is made by computing only the 573 most significant singular values of the SVD out of a possible 2592 (the number of cells) and using the 573 corresponding singular vectors to approximate R, i.e. $R = V_p V_p^T$. V_p is the rectangular 2952x573 submatrix of V where V is defined by the Lanczos decomposition of the full matrix $A = USV^T$.

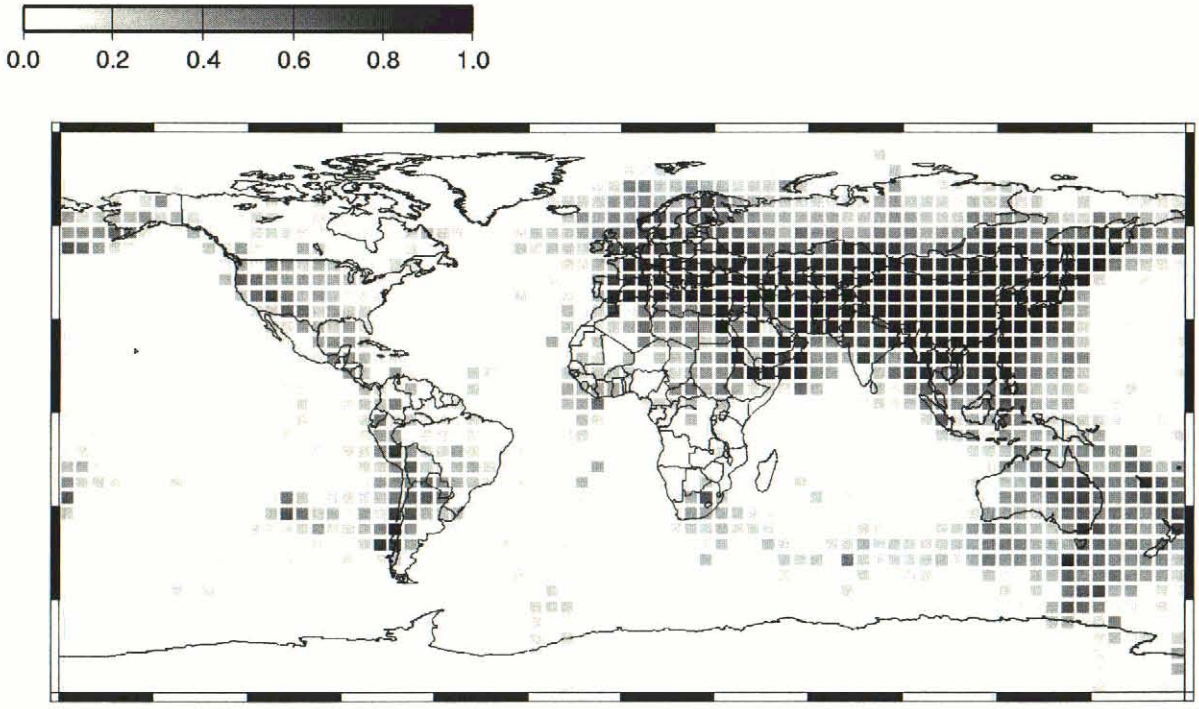

Figure 1. Map of the diagonal elements of the resolution matrix for group velocity measurements in the frequency range 0.025 to .0330 Hz using an approximation of the SVD using the Lanczos method and 573 out of a possible 2592 singular values.

2.5.2 Selection of new model types from resolution calculations.

We computed the resolution matrices for the 2D group velocity tomographies for eight frequency bands: below 0.01 Hz, 0.01 to 0.0140 Hz, 0.0140 to 0.0167 Hz, 0.0167 to 0.025 Hz, 0.025 to 0.033 Hz, 0.033 to 0.04 Hz, 0.04 to 0.05 Hz, 0.05 to 0.067 Hz. Those cells associated with diagonal components of resolution matrices greater than 0.6 for 8 frequencies were given new model types. The 0.6 value for a cell means that there is some smearing among other cells but that the true perturbation of the cell contributes the most (60%) to the tomographic value. The new types had the same number of layers and layer thicknesses as the originating types, and the initial parameters were set the same. In this example, the addition of these new model types increased the number of types from 230 to 388 and reduced the weighted standard deviation in data by about 5%.

2.6 Five Degree Models

Figures 2 through 5 show the dispersion curves for our best five degree model.

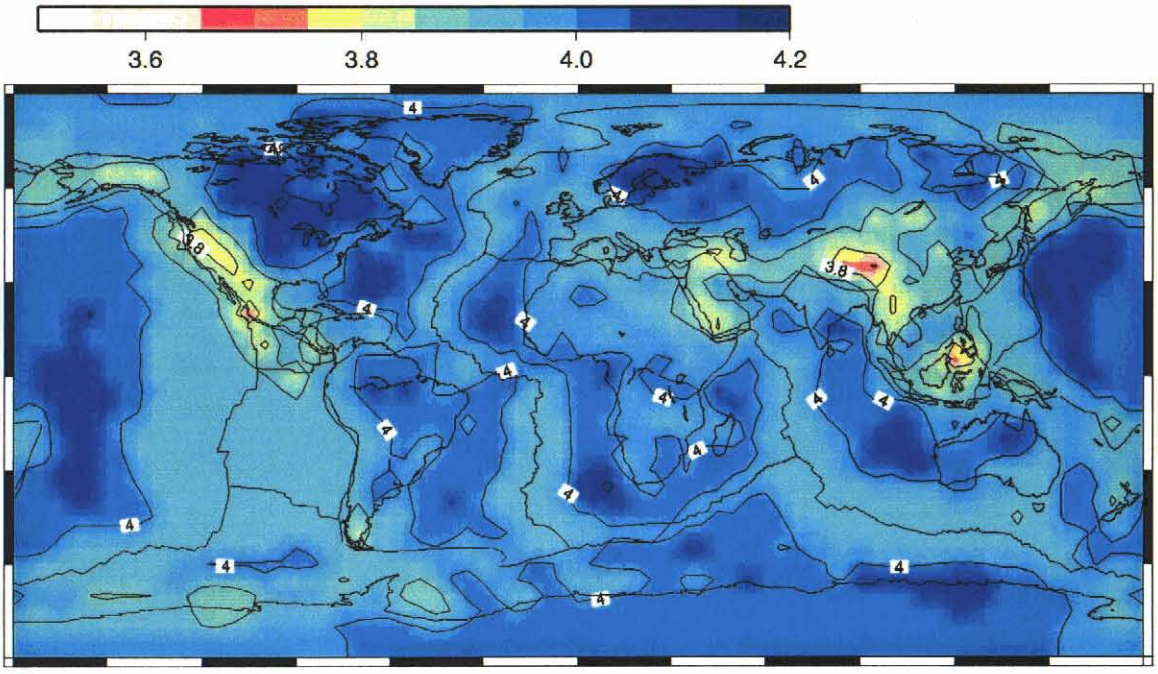

Figure 2. 50-second phase velocity.

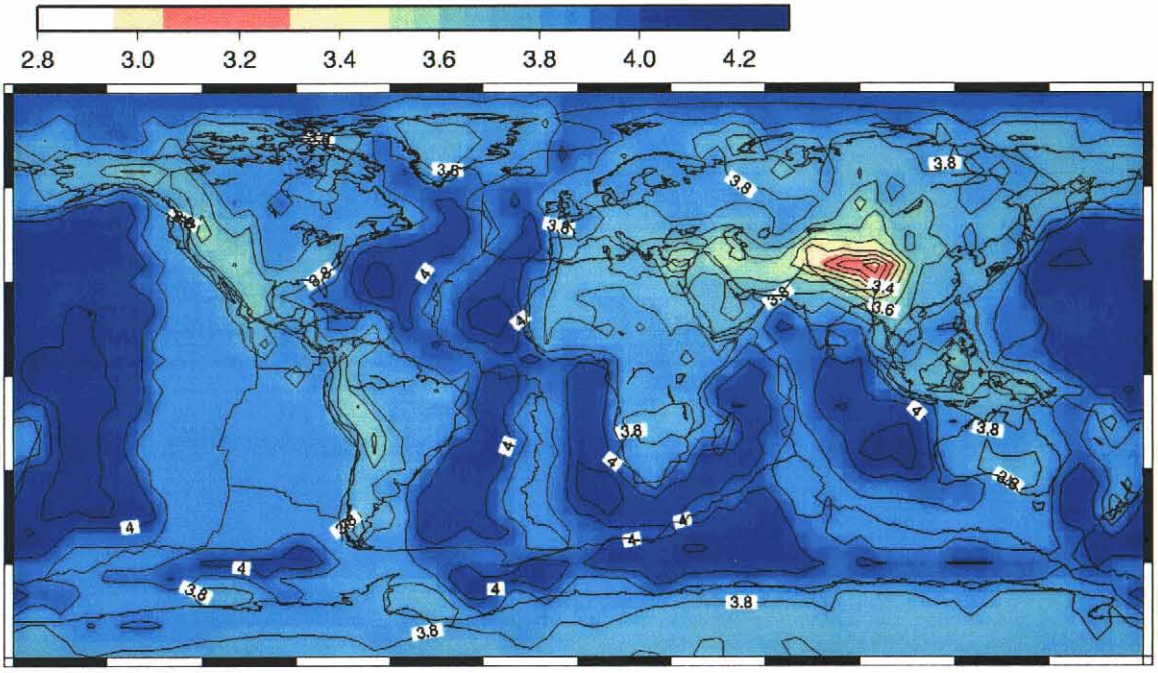

Figure 3. 50-second group velocity.

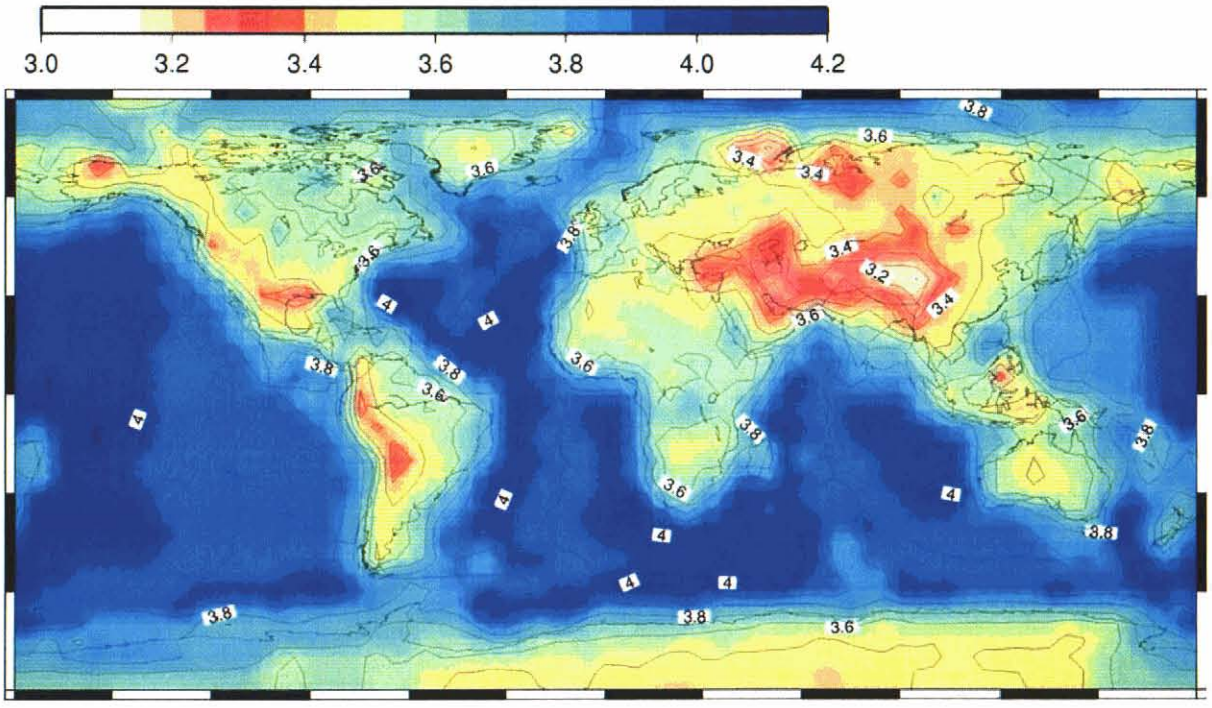

Figure 4. 20-second phase velocity.

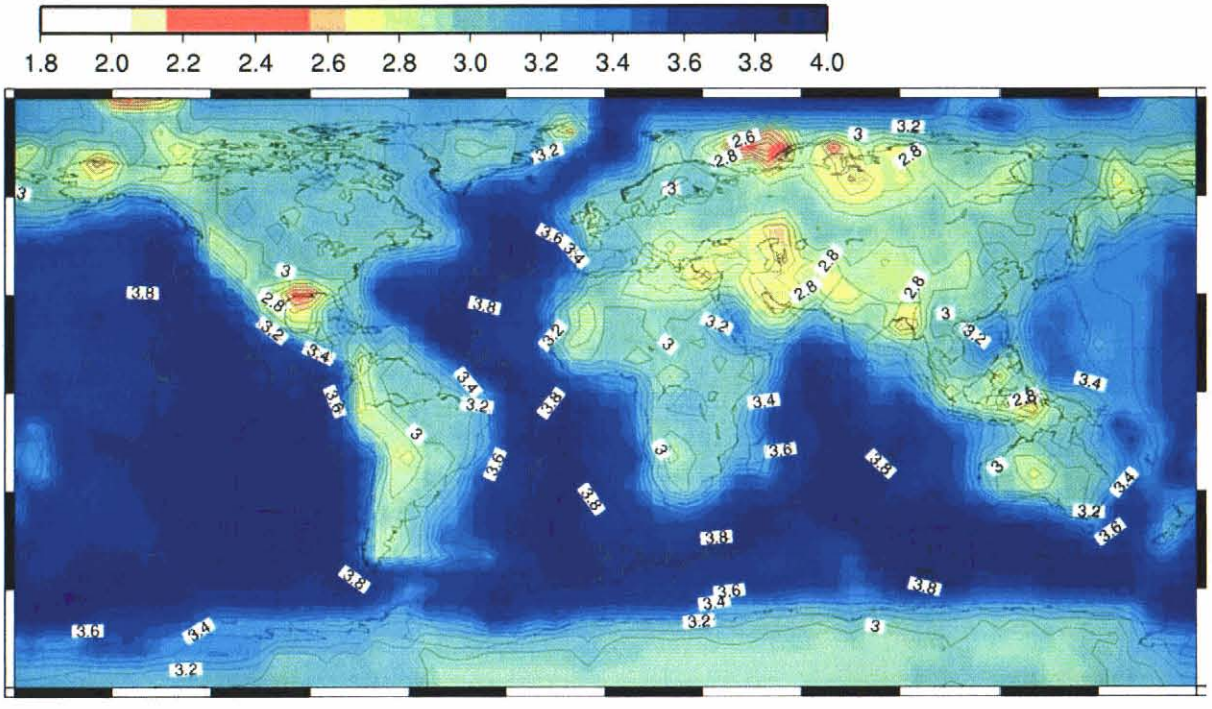

Figure 5. 20-second group velocity.

2.7 Inversion on a One Degree Grid

As discussed previously, for the one degree model, the inversion is performed for shear velocity structures in approximately 550 distinct crust and upper mantle model types, while the shallow structure, bathymetry, as well as small changes in layer thickness and Moho depth, can vary on a one degree grid (64,800 distinct models). P wave velocities are constrained via a constant Poisson's ratio of 0.27, and density via Birch's Law of $\rho = 0.65\beta + 400$ in where ρ is density and β is shear velocity in MKS units. The layers vary in thickness (averaging about 10 km) and reach down to a depth of about 300 km. Below 300 km the Earth model is fixed to match AK135. A continuity condition is applied between the deepest layer used in the inversion and the structure below. The top few km of the model (consisting of water, ice and/or sediments) are fixed and match data from 1 degree bathymetry maps made by averaging Etopo5 5 minute measurements of topography, and Laske and Masters (1997) 1 degree maps of sediments.

Our current preferred one degree model consists of 556 model types. There are two main varieties of model types, those originating from the Crust 2.0 2x2 degree crustal types (Bassin et al., 2000 and Laske et al. 2001) and those based on ocean ages (Stevens and Adams, 2000). The Crust 2.0 models are an improvement of the Mooney et al. (1998) Crust 5.1 model revised and refined to a 2-degree scale. Crust 2.0 consists of a 2-degree partition of the Earth with each cell having one of 341 crustal types. Each type consists of up to 8 layers: ice, water, up to two sedimentary layers, 3 crustal layers and an upper mantle layer. Vp, Vs, thickness, density and Q are specified for each layer. The 341 crustal types fall into 24 broad categories. Each of these categories consists of several types with the same crustal velocities, densities and Q, but differing in thicknesses of the layers, sedimentary structure, ice thickness and bathymetry.

Because many of the Crust 2.0 models differ only in shallow structure rather than crustal velocity, we use a somewhat different set of models. We combine similar model types that vary in shallow structure, since we treat those shallow variations as independent constraints. This has the effect of reducing the number of model types relative to Crust 2.0. However, we also separate models in widely separated regions so that results from a model in North America, for example, do not affect a model of the same type in Eurasia. This increases the number of model types. We also reparameterized the structure of the oceans based on ocean age. We formed 17 ocean types based on the Muller et al. (1997) isochron map. There are five types for each of the three major oceans: Pacific, Indian and Atlantic. The five types match the age ranges 0 to 10.9 Ma, 10.9 to 20.1 Ma, 20.1 to 40.1 Ma, 40.1 to 83.5 Ma and 83.5 to 180.0 Ma. The remaining two types are for the Arctic Sea for ages 0 to 40.1 Ma, and 40.1 to 180.0 Ma. Sedimentary structures, bathymetry and lateral boundaries between different oceanic types are included on a 1 degree level of detail. The mantle structure for our new parameterization comes from the 1997 version of AK135 (Kennett *et al.*, 1995). This parameterization serves as the initial model for a series of 3D tomographic inversions. Table 1 summarizes the new parameterization.

Table 1. Summary of the new Earth parameterization.

Model Element	Mantle structure Vp Vs and density	Moho depth	Thicknesses of 3 crustal layers	Crustal Vs,Vp, density, and Q	Sediments	Bathymetry	Ice
Vertical Resolution	~20 km up to max. depth ~ 300km	~1 km	~ 1 km	1-10 km	100 meters	100 meters	0.5 km
Horizontal Resolution	Variable:- average ~ 10 degrees.	2 degrees	2 degrees	Variable. Same as for mantle.	1 degree	1 degree	2 degrees
Parameter Origin	New parameter-ization	Crust 2.0	Crust 2.0	New parameter-ization	1 degree sed. map (Laske and Masters, 1997).	Etopo5	Crust 2.0
Inversion Role	Vs is free. Vp is constrained via fixed Poisson's ratio. Density via Birch's law. Q fixed.	fixed	fixed	Vs is free. Vp is constrained via fixed Poisson's ratio. Density via Birch's law. Q fixed.	fixed	fixed	fixed

2.8 One Degree Models

Figures 6 through 9 show phase and group velocity maps at 20 and 50 seconds for the final one degree model.

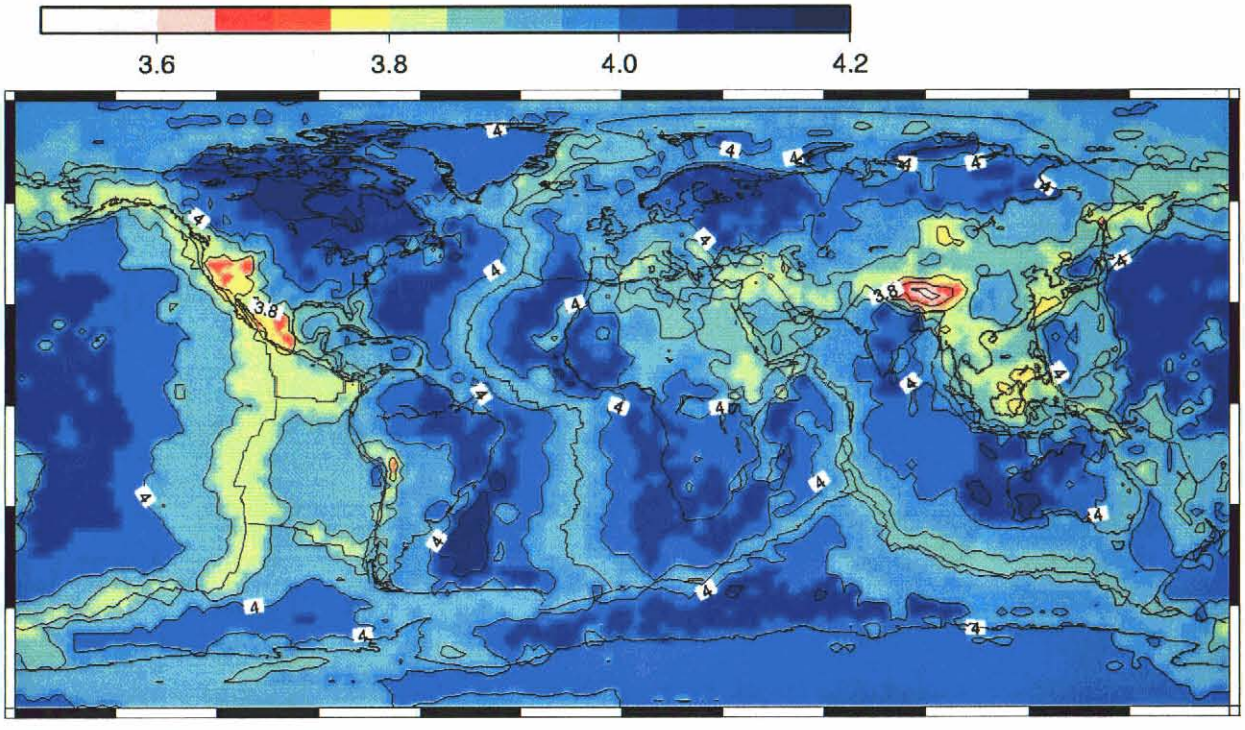

Figure 6. 50-second period phase velocity map.

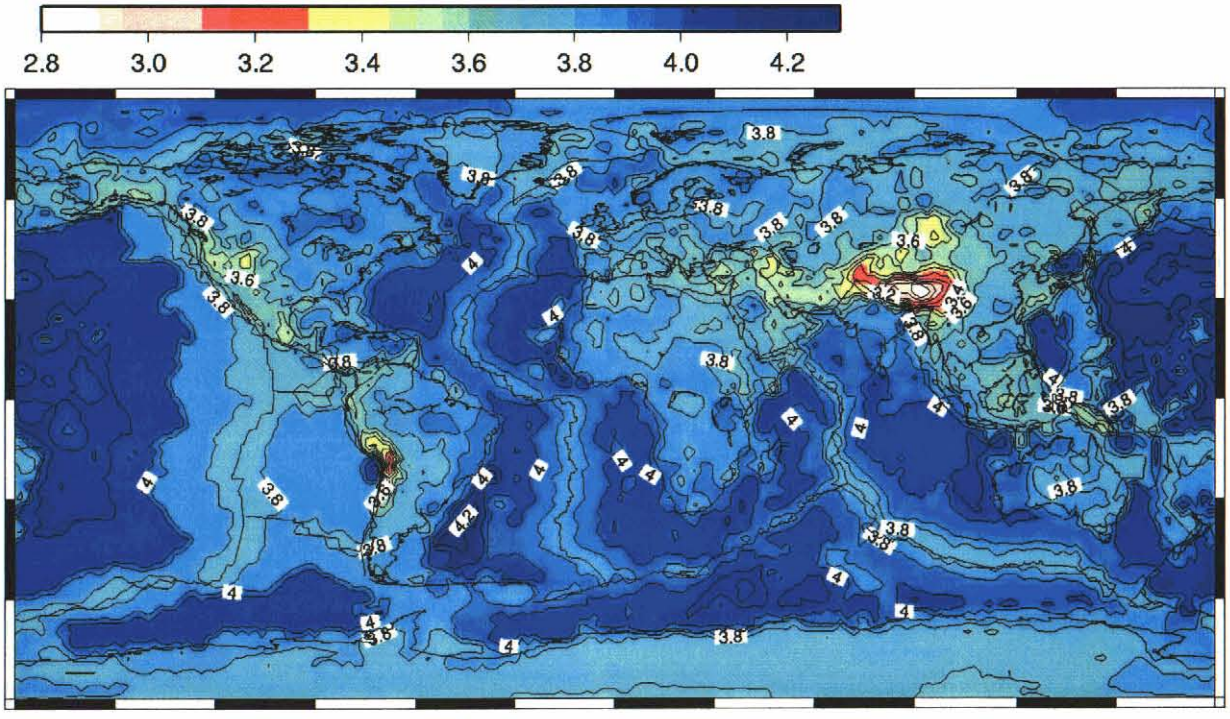

Figure 7. 50-second period group velocity map.

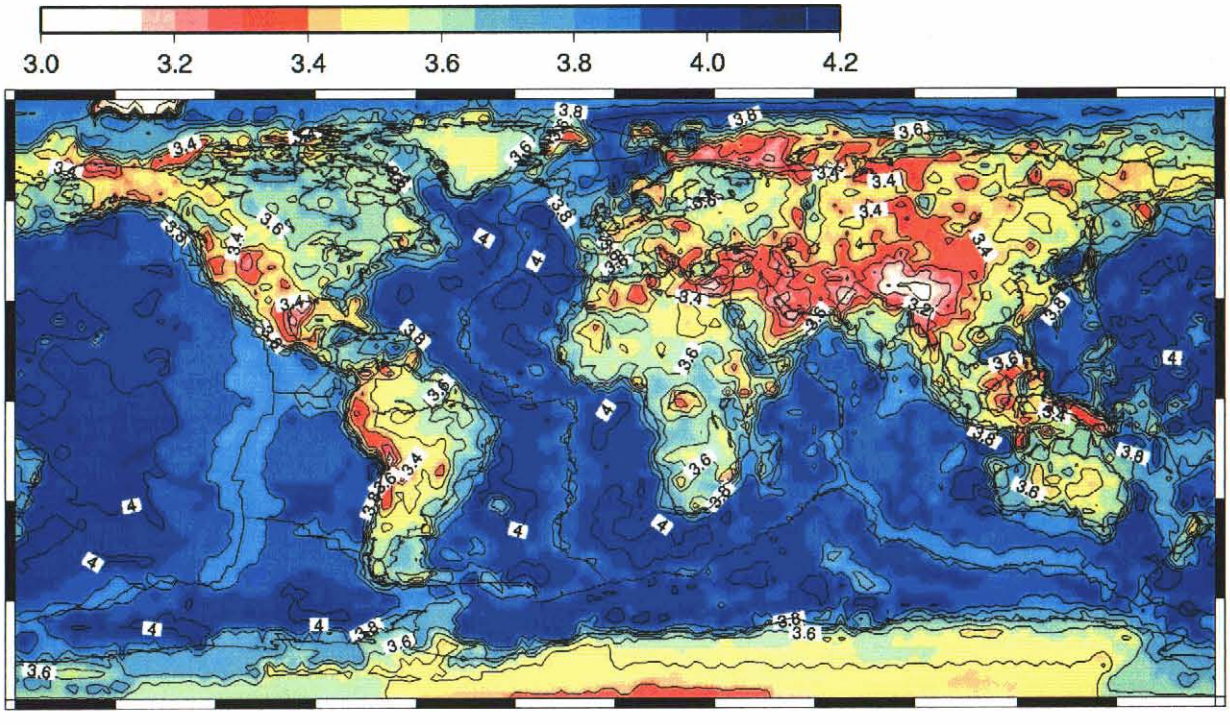

Figure 8. 20-second period phase velocity map.

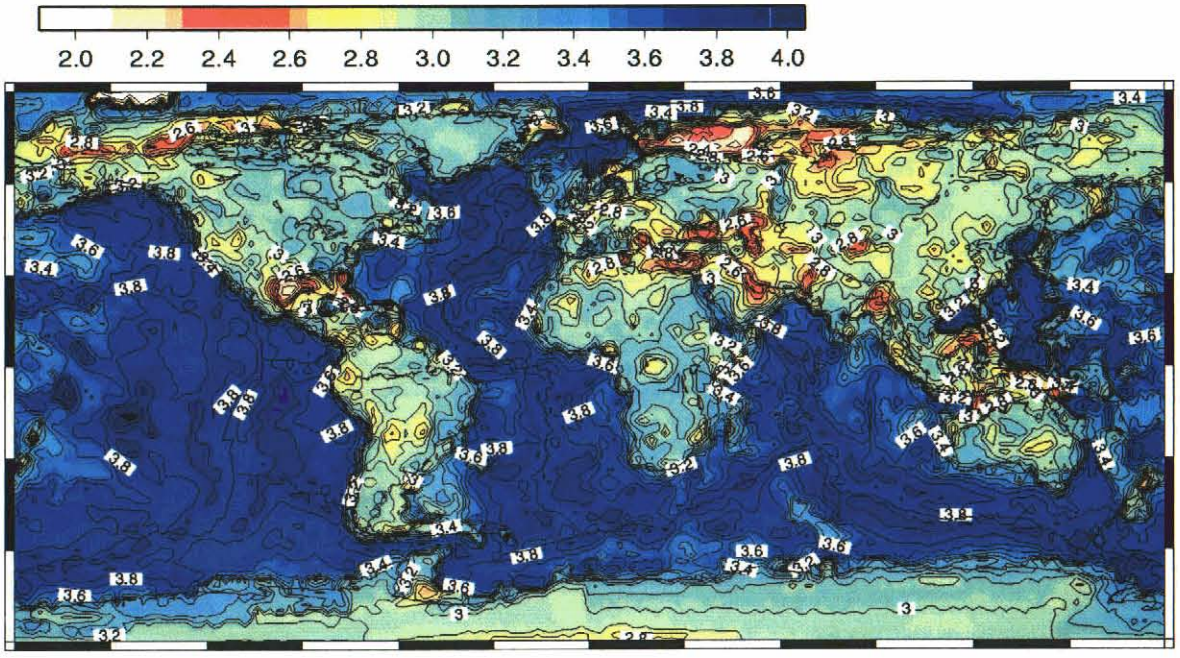

Figure 9. 20-second period group velocity map.

The shear velocity depth profiles of the three main oceanic types after tomographic inversion are shown in Figure 10. Note that the low velocity zone at ~80 km is deeper for younger structures, as we would expect, and that the structures found for each ocean are quite similar at the corresponding age even though inversions were performed independently.

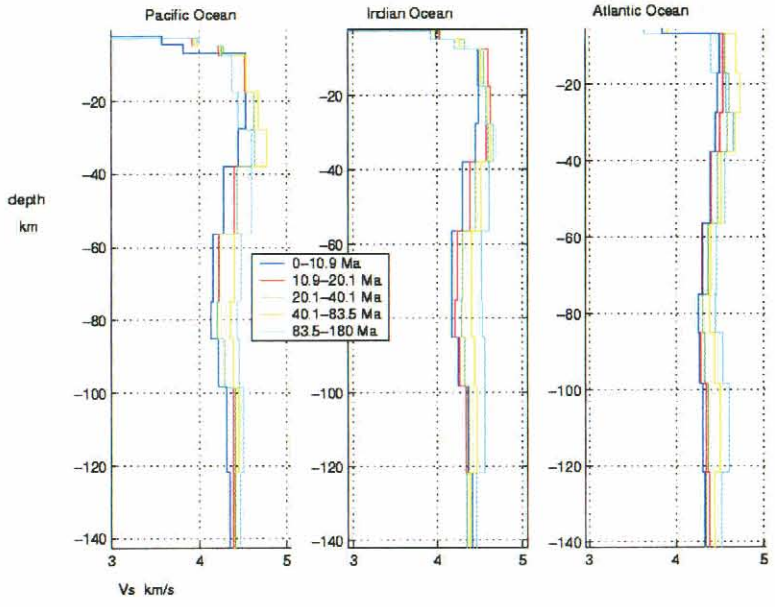

Figure 10. Shear wave velocity depth profiles for the main 15 ocean types. These results are consistent with thermal models of oceanic lithosphere.

Section 3
New Detection Algorithm Using Phase-Matched Filtering

Automatic identification of surface waves at the International Data Center is currently performed using the processing program Maxsurf by narrow-band filtering the data at several frequencies and then comparing the arrival times with a regionalized dispersion model. An automatic surface wave processing program, Maxpmf, has been developed which is similar to Maxsurf except that it applies phase-matched filtering to seismograms and calculates path-corrected spectral magnitudes in addition to M_s. Maxpmf integrates a regionalized phase velocity model to generate a phase-matched filter which is used to compress the surface wave waveforms. Figure 11 shows an example of waveform compression after application of phase-matched filters to a data set. Note that the signal is both compressed and enhanced relative to the background noise. We want to take advantage of the improved signal to noise ratio to improve surface wave detection, and have experimented with a number of ways to do this. The most obvious method, applying an STA/LTA detector to the compressed waveform does not work as well as the current IDC procedure.

A procedure that does work well, however, is to use essentially the same procedure currently used at the IDC, but to apply it to the phase-matched filtered waveform instead of the original waveform. The allowable time window has the same width as in the current procedure, but the predicted arrival time is now zero in all cases. Figure 12 shows the recommended way to perform surface wave identification using phase-matched filtering, which is to apply narrow-band filters to the phase-match filtered waveforms and the look for arrival times near zero.

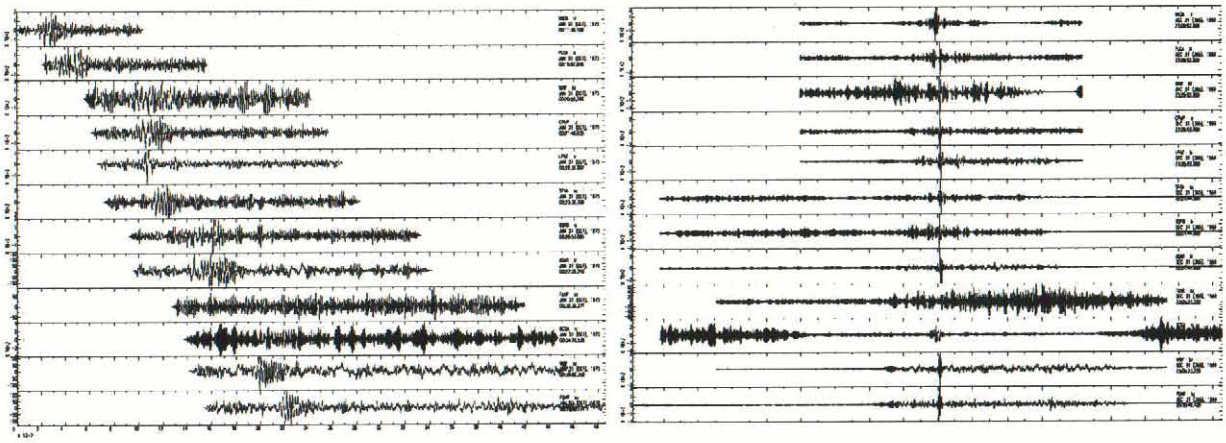

Figure 11. Data in the 5 km/sec to 2 km/sec time window from an m_b 3.9 South Pacific earthquake after transformation to a KS36000 instrument (left) and after compression by phase-matched filtering (right).

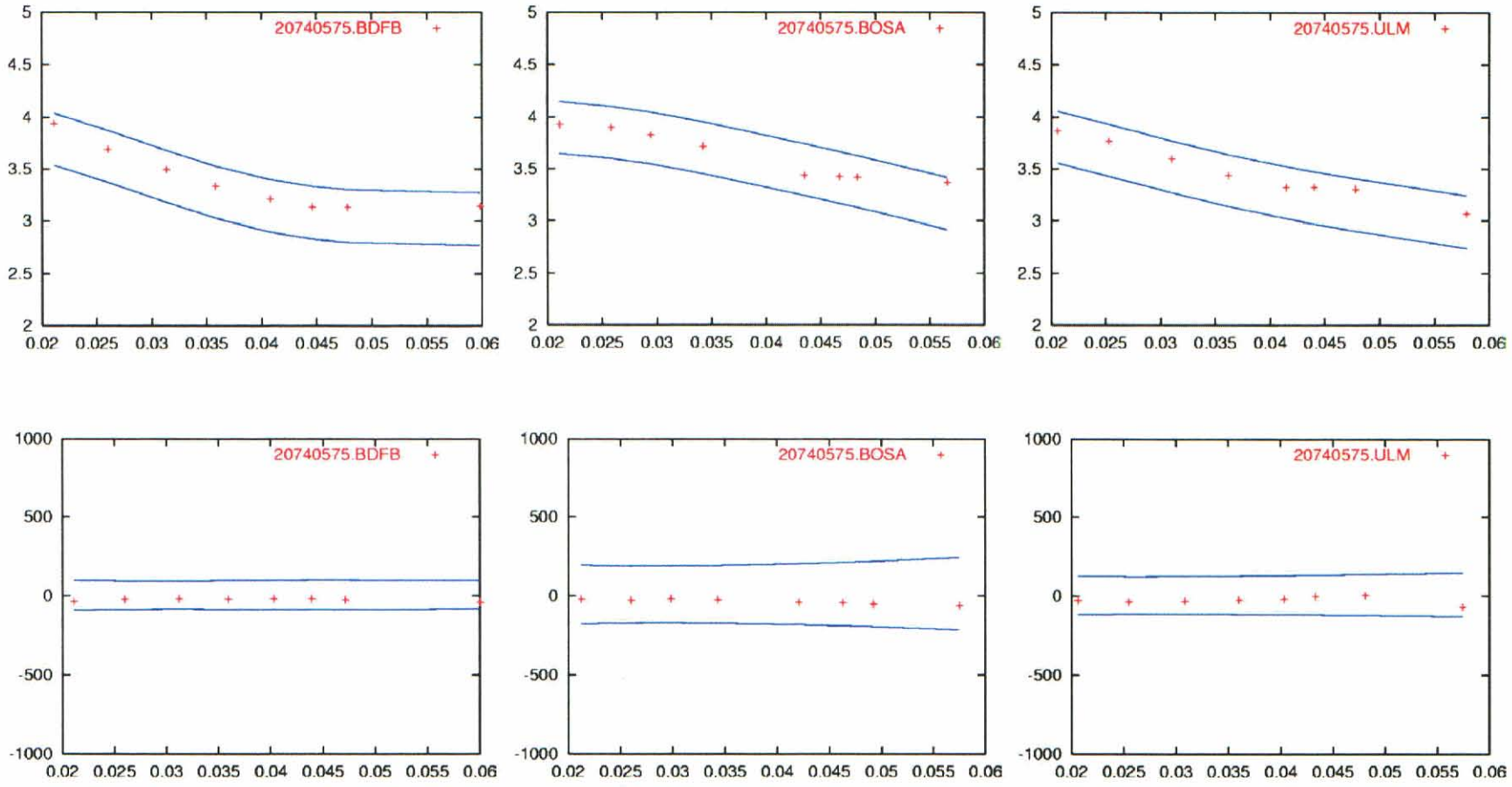

Figure 12. The narrow-band filter detection test (top) compares measured group velocity with a regionalized group velocity model. To improve detection, we phase-match filter the data first, and then apply narrow-band filters (bottom). The detection test is applied for the same time interval, but the time is now centered around zero. This example is for an m_b 4.2 South American earthquake observed at BDFB, BOSA, and ULM.

Section 4
Tests of Dispersion Models

4.1 IMS Data

As a test of both the improvement in models and the ability of phase-match filtering to improve detection, we ran Maxpmf on one full day of data and applied both the current narrow-band filtered test and the phase-matched filter test described above to this data set. The results are shown in Figure 13. The five bars show, respectively, the number of detections determined using IDC 5 degree model with the current IDC procedure, the number of detections using the best 5 degree model, the number of detections using one of the early one degree models, the number of detections using this same one degree model with phase-matched filtering, and detections using a more recent one degree model. Each improved model, and the implementation of phase-matched filtering, shows an improvement. The number of detections increased by 40% over current IDC detections with phase-matched filtering using the recent one degree model. The first one degree model used in this test was a modification of the earlier 5 degree model, and did not include the modifications discussed earlier to incorporate the Crust 2.0 improvements.

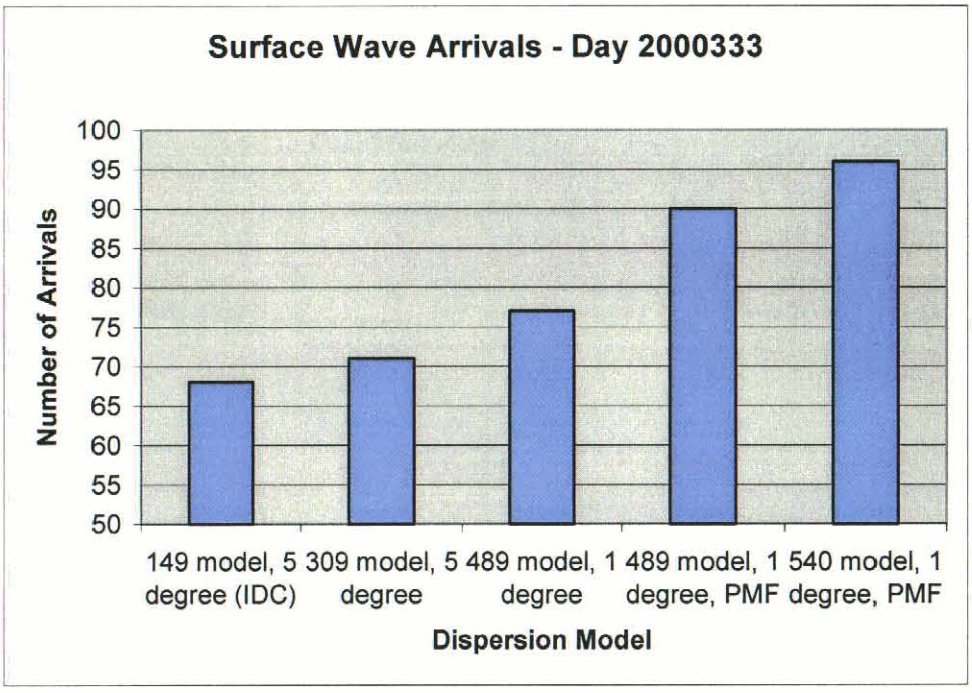

Figure 13. Improvement in the number of detections for a day of data with improvements in the model, and with phase-matched filtering.

4.2 Nuclear Explosion Data

As a second test, we examine the ability of the model to predict dispersion of surface waves from explosions at historic test sites. Part of the dispersion data set used in our surface wave study consists of data from these test sites. Specifically, we are using surface wave dispersion from path corrections generated by analysis of multiple surface waves from test sites (Stevens, 1986) as well as dispersion data measured by Yacoub (personal communication). The ability to predict this data is a good consistency check on the global earth model. Tables 2 and 3 show the average and standard deviations of the group velocity residuals for 5 major test sites, and shows how they have changed with expansion of the data sets and improvement in the models.

Table 2. 40-second group velocity % average residuals (Standard Deviations).

Source	IDC 5° 149 Models	5° 388 Models	1° 556 Models
NTS (59)	0.14 (1.40)	0.20 (1.17)	0.19 (1.17)
East Kazakh (40)	0.75 (2.14)	0.34 (1.15)	0.41 (1.00)
Mururoa (13)	-0.81 (1.47)	-0.86 (1.88)	-0.47 (1.77)
Novaya Zemlya (94)	-0.31 (1.68)	-0.37 (1.53)	0.28 (1.62)
Amchitka (55)	0.23 (1.36)	0.43 (1.13)	0.44 (1.18)

Table 3. 20-second group velocity % average residuals (Standard Deviations).

Source	IDC 5° 149 Models	5° 388 Models	1° 556 Models
NTS (58)	-0.52 (2.29)	-0.22 (1.80)	-0.46 (2.29)
East Kazakh (40)	-0.79 (2.00)	-0.51 (1.46)	0.08 (1.30)
Mururoa (11)	0.39 (1.44)	0.50 (1.57)	-0.34 (1.50)
Novaya Zemlya (99)	-0.39 (3.55)	-0.18 (2.92)	0.01 (3.31)
Amchitka (54)	0.70 (3.51)	0.66 (3.10)	0.22 (3.58)

Although both the best 5 degree model and the one degree model are significant improvements over the IDC model, results are mixed for the best 5 degree model versus the one degree model. This is surprising considering the significant improvement in detection capability discussed in the last section and overall improvement in data fit. A number of the long oceanic paths are actually worse in the 1 degree model, in spite of the improvement in accuracy of ocean

modeling. Consequently, we have reviewed the surface wave data to identify the reasons for the remaining data misfit. Specifically, we are looking for the following:

1. Errors in the data. Some of the data was well constrained by multiple signals recorded on digital instruments, however some of the measurements are based on a single or small number of hand-digitized waveforms. Some of these measurements therefore may not be accurate.

2. Consistent differences between the predicted and observed dispersion indicating errors in the model. This indicates that the inversion needs improvement, which can be accomplished by improvement of starting models, or creation of additional model types.

3. Paths that cannot be modeled adequately by the great circle approximation. There appear to be only a few of these, and they consist primarily of long, grazing paths along continental/ocean boundaries. Figure 14 shows an example of waveforms on the path from NTS to MAJO. There are three distinct arrivals that consistently occur for each event. The second arrival corresponds well to the predicted great circle arrival time, however there is a larger first arrival which apparently takes a faster oceanic path. Figure 15 shows the great circle path from NTS to MAJO.

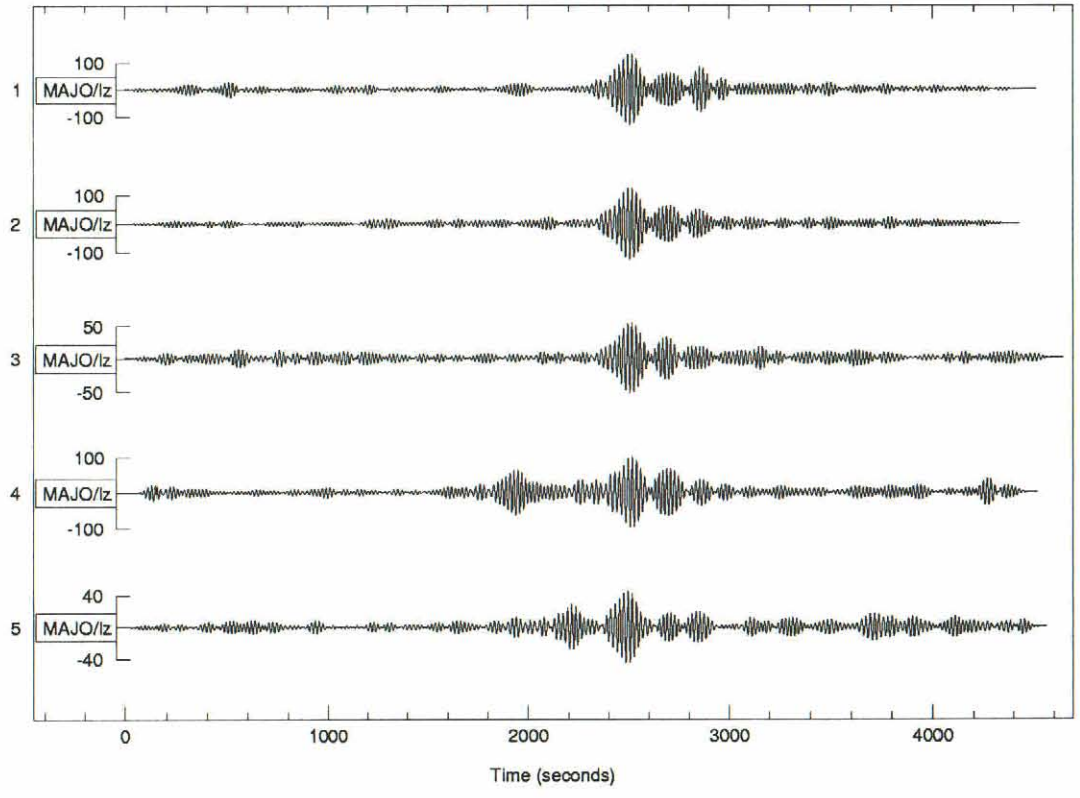

Figure 14. Surface waves recorded at MAJO from 5 NTS explosions bandpass filtered near 20 seconds.

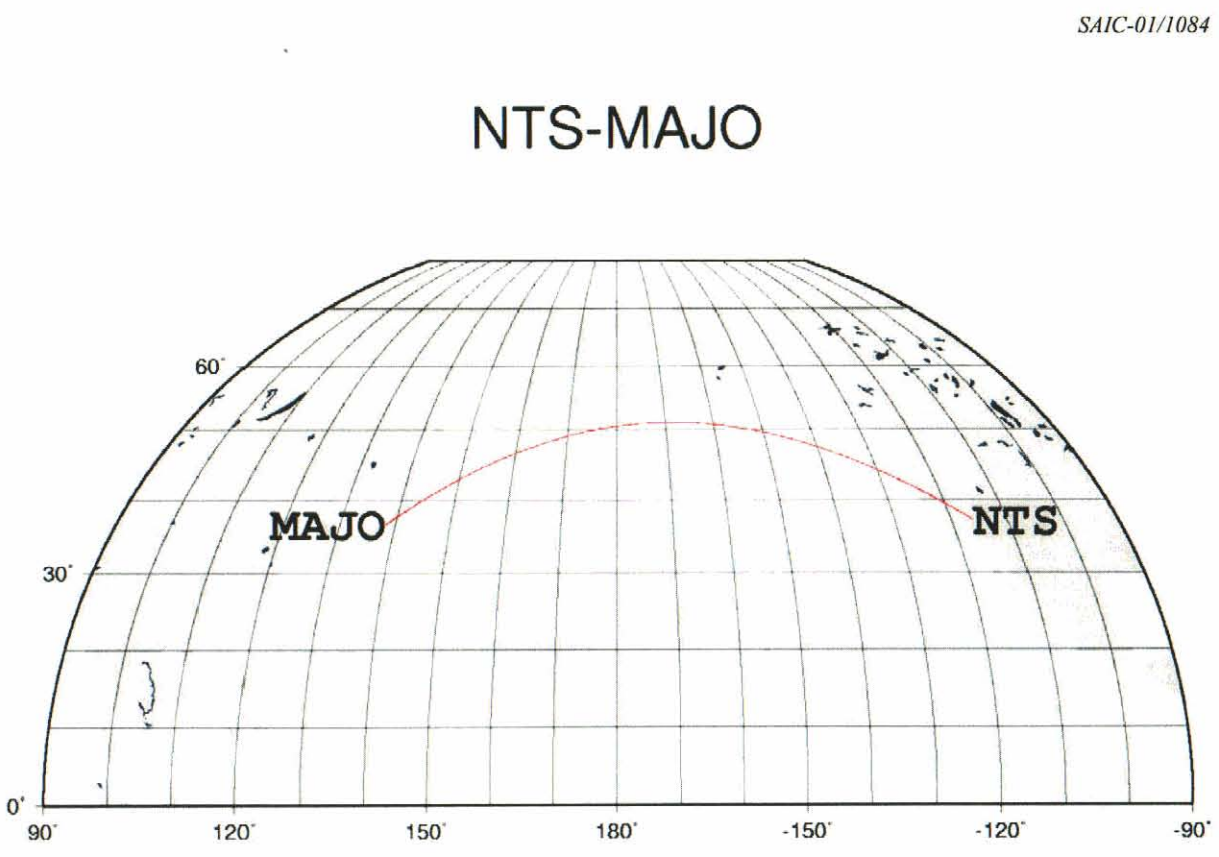

Figure 15. The great circle path from NTS to MAJO is a grazing path along the northern boundary of the Pacific Ocean.

In order to improve the predictive ability of the global models for these paths, we recommend the following changes for future work:

1. Remove or correct erroneous data. There are four common types of errors that occur. First, the measurement may be inaccurate because of a poor quality waveform. In this case the measurement cannot be corrected and should be removed. Second, the data may be good, but the measurement inaccurate for any of a variety of reasons. In this case the measurement should be corrected if possible, removed otherwise. Third, in the case of phase-velocity the wrong phase-velocity branch may have been selected. Particularly for more distant stations the phase velocity branches (calculated from phases that differ by multiples of 2π) can be difficult to determine. The improved predictive capability of the models makes it possible to verify or correct the phase velocity in some cases. Fourth, the data may be accurate over a fixed frequency band but inaccurate in some range. There are two principal cases where this occurs. First, particularly with hand digitized data, the group velocity cannot be measured accurately, most commonly at the lowest or highest frequencies. Second, in the case of oceanic paths, an averaged path may have extended into the frequency band where the dispersion curve drops rapidly. This typically happens only at the highest frequencies (> 0.05 Hz).

2. Improve starting models. As discussed previously we are using Crust 2.0 as a starting model and constraint on the inversion. That is, the inversion tries to minimize the data misfit together with the misfit between the model and the constraining model. So to the extent that the starting models can be made more realistic the inversions will improve. One way to accomplish this is to use the inversion results to replace starting models in regions that are well constrained by the data while retaining Crust 2.0 in other regions, or to perform more detailed manual inversions of subsets of data corresponding to particular regions of interest.

3. Remove data that cannot be predicted adequately using great circle paths. As discussed above, some surface wave arrivals cannot be adequately predicted by using the approximation that the surface wave follows a great circle path. For most paths this is a second order effect because although the surface wave follows whatever path takes the shortest time, any faster non-great circle path will also be longer. So, for example, if the surface wave follows a path that is 5 % faster and 4% longer than the great circle path, the travel time change is only 1%. For cases such as grazing paths on ocean continent boundaries, however, the effect can be large. It may be possible to correct for these anomalous paths using non-great circle ray tracing, however the predictive capability of these algorithms needs to be evaluated, otherwise predictions overall could be degraded. The recommended approach for now is to document these anomalous paths and remove them from the data set.

Some of the errors discussed here had little effect on earlier inversions because the results were not accurate enough to resolve these differences, but now that dispersion predictions from the inversion models are becoming accurate to within about one percent for many paths, errors of a few percent in the data can significantly degrade the results. Further improvement will therefore require reviewing the data set, removing erroneous values, and adding new higher quality data points where they are needed.

Section 5
Use of Surface Waves to Improve Location

Surface wave arrival times can be used in the same manner as (or together with) P-wave arrival times to determine source location. With a good regionalized group velocity model and well determined group arrival times, the location could be determined quite accurately, and in cases where P-wave coverage is poor, or azimuthal coverage is limited, using surface wave arrivals has the potential to significantly improve location accuracy. Yacoub (2000) found that he was able to determine the location of 7 NTS explosions more accurately with surface waves narrow-band filtered in the 17 – 23 second period band than with P waves. This was done using a constant group velocity of 3.0 km/sec to determine location for all paths. This result is attributed to the fact that surface wave group velocities are much slower than P-wave velocities, so that errors in arrival time correspond to significantly smaller errors in distance than the corresponding errors in P wave arrival times, and to the consistency in surface wave arrival times.

We have performed some experiments using our global group velocity models and dispersion measurements to assess the ability to locate events using surface wave arrivals. Table 4 lists location errors from Yacoub (2000) derived using both surface waves and P waves, and the location errors we derived from independent measurements of data at several frequencies from the same events using the regionalized dispersion curves discussed earlier. The results confirm that location estimates are somewhat better than can be obtained from P-wave arrivals at the same stations, although the location errors are slightly larger than obtained by Yacoub. This may be because Yacoub used a larger and higher quality data set. Also, it should be recognized that Yacoub's P-wave measurements used only data from stations that also had surface wave data, and considerably better results could be obtained from a larger P-wave data set. ISC locations for these events, based on all available P-wave measurements, have errors on the order of just a few kilometers.

Yacoub (2000) found remarkably constant group velocity measurements, all very close to 3.0 km/sec. We cannot confirm this and assume that it must be due either to a particular choice of paths, or some anomaly in the way the measurements were made. Figure 16 shows the distribution of measured group velocities from all of the explosion data from all test sites. While the mean of the distribution is very close to 3.0 km/sec, there is considerable variation from this value in the data set.

Table 4. Location errors for 3 methods and the number of stations used for each (Yacoub P and surface wave locations used identical sets of stations).

Event	# STA		Location Error (km)		
	Yacoub	IDC	Yac. LR	Yac. P	IDC LR
Hearts	19	17	11.2	18.3	22.5
Backbeach	19	2	9.7	33.1	NA
Scantling	18	11	25.1	49.9	18.9
Lowball	17	12	16.3	28.3	18.1
Mizzen	14	9	9.8	32.0	34.2
Strake	14	0	13.0	26.0	NA
Sheepshead	12	16	9.2	16.1	13.0
Averages			13 ± 6	29 ± 11	21 ± 7

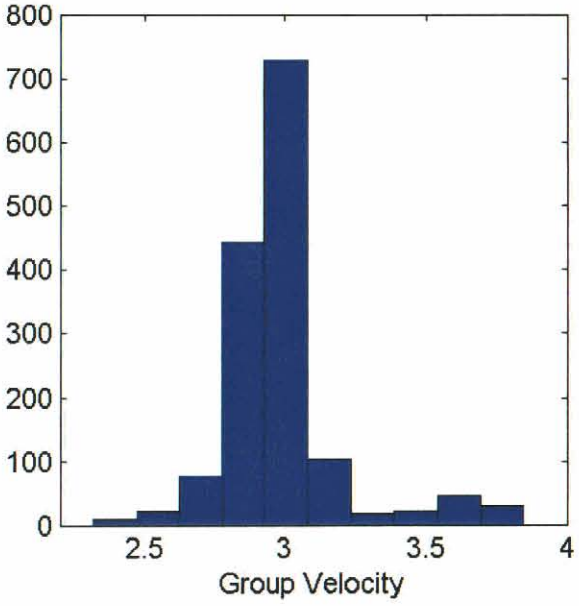

Figure 16. Histogram of measured group velocities of 20 second Rayleigh waves from explosions at all major test sites.

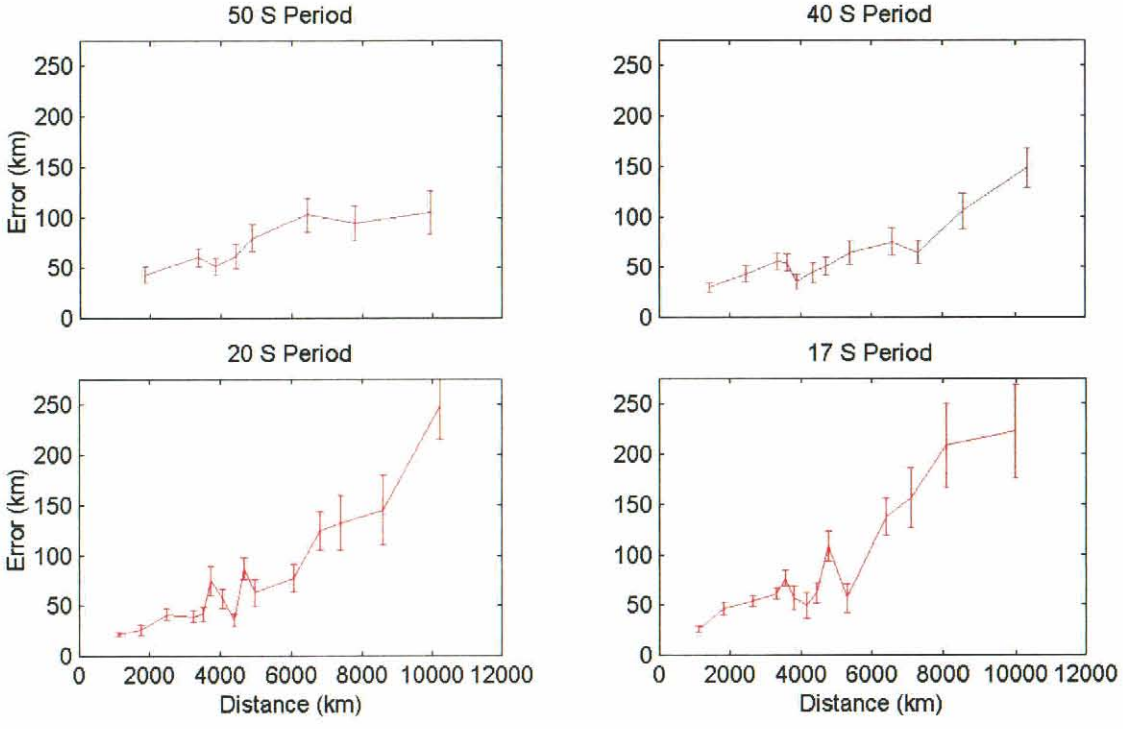

Figure 17. Mean and two standard deviation error bounds of distance estimates from single stations, for different frequencies. There are approximately 100 data per distance bin.

Figure 17 shows the estimated error as a function of distance for single station measurements. In general, the location error increases with distance to the observing station. Lower frequencies, however, degrade much more slowly. However, at shorter distances higher frequency data gives more accurate locations.

Figure 18 shows the location error derived from surface wave measurements from Semipalatinsk test site explosions as a function of the number of recording stations. The results are similar at NTS, with a typical location error of about 30 km. It is important to note, however, that location accuracy depends as much or more on which stations recorded the event as on how many. Referring to Figure 17, it is clear that surface waves recorded at distances of 3000 km or less provide much better constraints on location than more distant stations. Surface waves are most likely to be useful in constraining location therefore when they are measured at shorter distances and combined with a small number of P-wave measurements. The P-wave measurements on their own may not be very accurate, but even a single surface wave accurately measured at a distance of <2000 km could significantly improve the location.

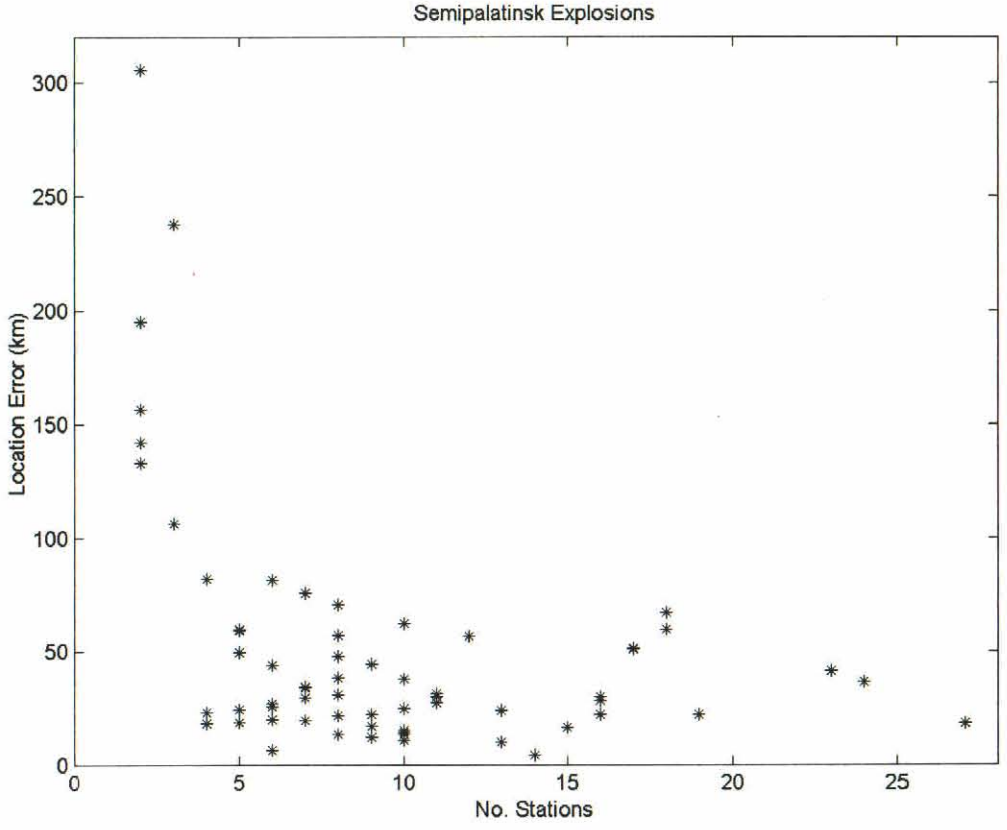

Figure 18. Location errors for Semipalatinsk explosions. The median error for events recorded at 6 or more stations is 30 km.

Section 6
Definition of M_s and Path Corrected Spectral Magnitudes

One of the principal motivations for this project is to improve the effectiveness of the M_s:m_b discriminant (Figure 19. See also Stevens and Day, 1985; Douglas *et al*, 1971; Marshall and Basham, 1972) by reducing the threshold for which surface waves can be detected and accurately measured.

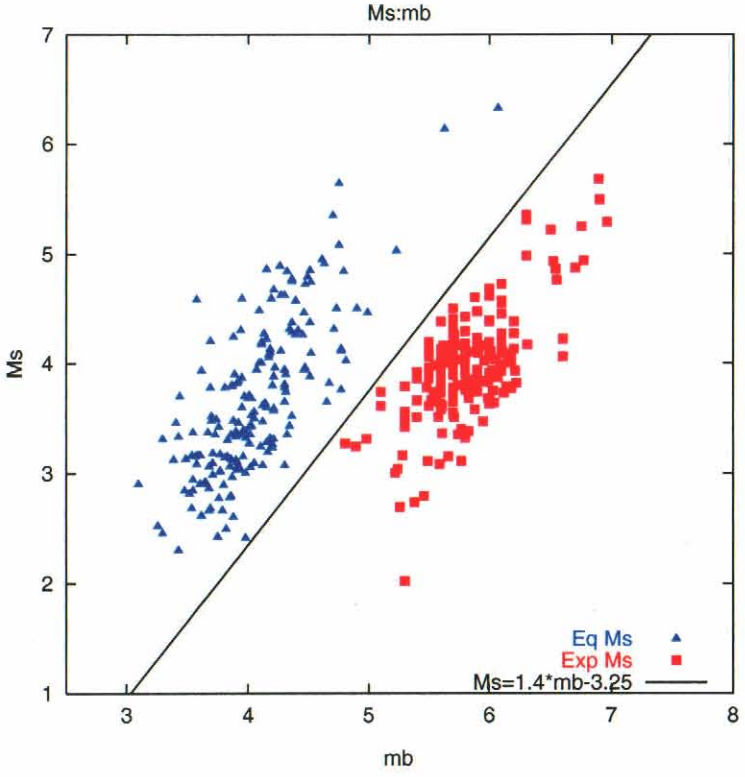

Figure 19. M_s:m_b plot for a data set of earthquakes recorded at the PIDC and historical explosions.

In addition to detection, it is also important to be able to measure the surface wave accurately, and it is important for the surface wave magnitude to be determined in a way that is as free as possible from regional biases and variations due to the frequency and distance at which it is measured. The definition of M_s adopted by IASPEI[1] is

$$M_s = \log(A/T) + 1.66\log\Delta + 0.3 \qquad (3)$$

where A is the instrument corrected zero to peak amplitude in nanometers, Δ is the source to receiver distance in degrees, and T is the period at which A is measured, with T measured near

[1] International Association for Seismology and Physics of the Earth's Interior.

20 seconds. NEIC[2] uses the IASPEI formula measuring A from the vertical component of a long period seismogram and selecting the largest amplitude for periods between 18 and 22 seconds. The factor of 1.66 in Equation 3 is intended to correct for a worldwide average surface wave attenuation rate, although a number of studies (e.g. Marshall and Basham, 1972) have shown that this in incorrect at distances less than 30°. Rezapour and Pearce (1998) recommended redefining M_S as

$$M_s = \log A/T + k \log \Delta + \tfrac{1}{2} \log(\sin \Delta) + \gamma \Delta \log e + D \qquad (4)$$

which is based on the theoretical formula for surface wave attenuation, with $k = 1/3$ and $\gamma = 0.0105$. The constant $D = 2.484$ makes this definition of M_S equal to IASPEI M_S at 83°. Equation 4 is now used as the standard magnitude definition at the IDC.

M_S as defined in Equations 3 or 4 can be quite variable at different stations because of differences in dispersion and attenuation along the travel path. Also, it is difficult to reliably measure a 20 second amplitude from a time domain waveform at distances less than about 20 degrees. Because of this, a number of authors have suggested modifications to make M_S more consistent. Marshall and Basham (1972), for example, derived a distance correction with a smaller slope at shorter distances, and empirical frequency dependent corrections to the amplitude depending on the type of earth structure between the source and receiver. Note that Equation 4 can be regionalized by varying γ and D as a function of location, and it can be made to work at periods other than 20 seconds by making γ and D frequency dependent. However, any time domain magnitude suffers from two problems: the difficulty of measuring a time domain waveform at a specific frequency, particularly at regional distances; and the variability of the k factor in Equation 4 which depends on whether the measured surface wave propagates with normal dispersion or as an Airy phase.

6.1 Spectral Magnitudes and Scalar Moment

The key to developing a surface wave magnitude that is regionalizeable, and gives consistent values at regional and teleseismic distances and in different frequency bands, is to use the equation for surface waves in a plane-layered structure to correct the spectrum. This equation can be factored into functions that depend on the source and receiver earth structure and the phase velocity and attenuation integrated over the path. The displacement spectrum for a Rayleigh wave at distance r from an *explosion* is given by:

$$U(\omega,r) = M_0' \frac{S_1^x(\omega,h_x) S_2(\omega) \exp[-\gamma_p(\omega) r + i(\varphi_0 - \omega r / c_p(\omega))]}{\sqrt{a_e \sin(r/a_e)}} \qquad (5)$$

S_1^x depends on the source region elastic structure and the explosion source depth. S_2 depends on the receiver region elastic structure, γ_p is the attenuation coefficient that depends on the attenuation integrated over the path between the source and receiver. c_p is the phase velocity integrated over the source to receiver path. φ_0 is the initial phase of the source. a_e is the radius of

[2] National Earthquake Information Center of the U. S. Geological Survey.

the earth. $M_0^{'} = \frac{3\beta^2}{a^2} M_0$ where M_0 is the explosion isotropic moment. This definition is introduced so that the function S_1^x does not depend explicitly on the material properties at the source depth.

We can use Equation 5 to define a spectral magnitude corrected for distance and spectral shape. We define, for any event, earthquake or explosion, the path corrected spectral magnitude, or scalar moment:

$$M_0^{'} = \left| U(\omega, r, \theta) \Big/ \frac{S_1^x(\omega, h_x) S_2(\omega) \exp[-\gamma_p(\omega) r + i(\varphi_0 - \omega r / c_p(\omega))]}{\sqrt{a_e \sin(r / a_e)}} \right| \tag{6}$$

Although the imaginary part of the exponential is removed by the absolute value, it is shown here explicitly because in practice the phase is used to generate a phase-matched filter to compress the signal and improve signal/noise ratio prior to taking the spectrum. The spectrum is then averaged over a frequency band to smooth the spectrum and get a stable measurement.

For an isotropic explosion source at depth h_x, $M_0^{'}$ is constant. Equation 6 therefore corrects completely for all frequency dependent and distance dependent factors. Using $M_0^{'}$ or $log(M_0^{'})$ as the definition of a new type of magnitude, the magnitude value will, ideally, be identical when measured at any distance range and over any frequency band. For an earthquake with double couple moment M_q, $M_0^{'}$ is given by:

$$M_0^{'} = M_q \left| S_1^q(\omega, h_q, \theta) / S_1^x(\omega, h_x) \right| \tag{7}$$

where S_1^q depends on the double couple orientation and depth, takeoff azimuth θ and source region elastic structure. In general $M_0^{'}$ for an earthquake is not completely frequency independent, but it is partially corrected for frequency dependence by removal of the path attenuation and receiver structure and similarities in the explosion and earthquake excitation function in the same source region. The remaining differences mean that the earthquake magnitude will vary somewhat when measured over different frequency bands while the explosion will not. In particular the spectra of deeper earthquakes will decline more rapidly with increasing frequency (This is a potential discriminant that is investigated in the following section). By defining the scalar moment with Equation 6, we obtain a measure of surface wave magnitude that is independent of range, nearly independent of frequency, and regionalizeable. The functions S_1^x and S_2 depend only on the source and receiver points and can be stored in a simple lookup table. The functions γ_p and c_p depend on the source to receiver path and can be found by integrating along a great circle path between the source and receiver in a regionalized earth model. Note that $log(M_0^{'})$ is equivalent to M_s, except that the distance correction is replaced by regionalized corrections and the spectral amplitude is obtained directly from the spectrum instead of measuring a time domain amplitude and estimating the frequency. M_s and

$log(M_0')$ are related approximately by $log(M_0') \approx M_s + 11.75$. Figure 20 shows $log(M_0')$ plotted vs. m_b for a set of IDC data and historical explosion data equivalent to Figure 19 for M_s:m_b. Here $log(M_0')$ was calculated using a frequency band of 0.02-0.05 Hz for all data.

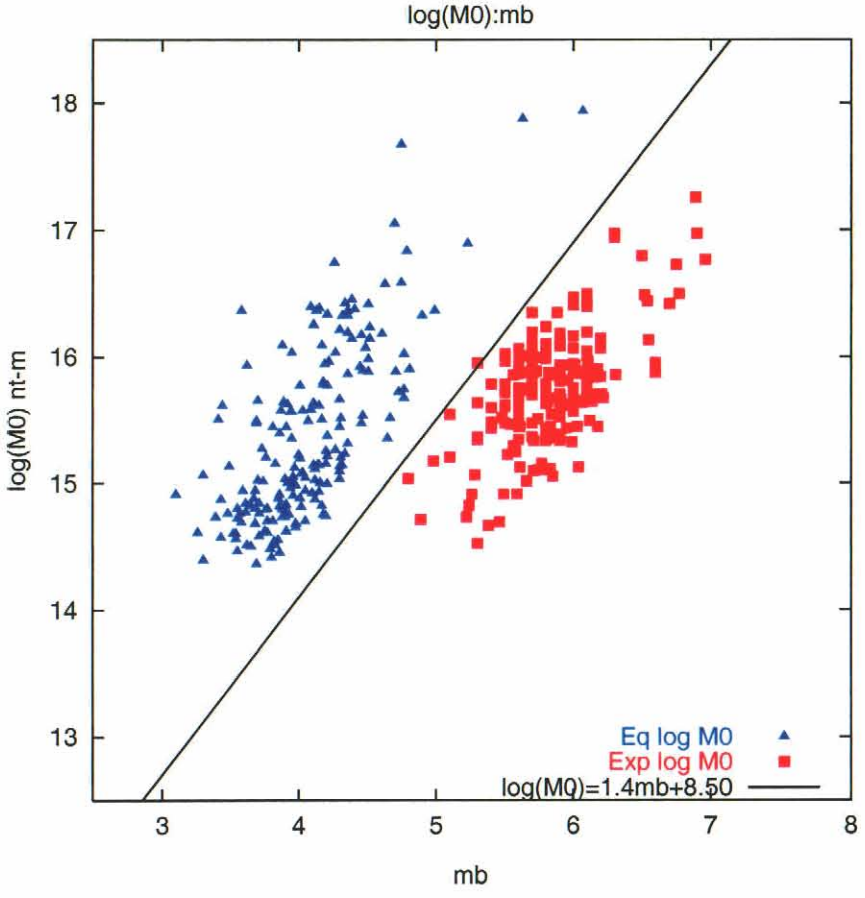

Figure 20. Log M_0:m_b plot for a data set of earthquakes recorded at the PIDC and historical explosions.

6.2 Regionalization

Equation 6 requires regionalized source and receiver functions and attenuation coefficients. While the phase velocity is not required to calculate scalar moment, it can also be regionalized and used to construct a phase-matched filter. Complete regionalization therefore consists of the functions S_1^x, S_2, γ, c, and u (group velocity) evaluated and stored for each grid block over the range of frequencies of interest. These functions have been calculated for all of the earth models developed under this project and are part of the data distribution which is described in Appendix A.

Section 7
Depth Discrimination Using Surface Wave Spectra

The idea of using spectral shape as a discriminant was first suggested by Tsai and Aki (1971) based on observations of small earthquakes and explosions on and near the Nevada Test Site. The theoretical basis for this is Equation 6, which is flat for explosions but not flat for earthquakes. In particular, the spectra of surface waves from earthquakes are predicted to fall off more rapidly at higher frequency because of the typical earthquake's greater depth. This effect also trades off with the effectiveness of the M_s:m_b discriminant for higher frequency regional surface waves. A shallow earthquake will most likely be identified as an earthquake by the M_s:m_b discriminant, while a deeper earthquake may fail the M_s:m_b discriminant when using a high frequency M_s, but may still be identified as an earthquake on the basis of its spectral shape. The excitation function ratio, Equation 6, is shown in Figure 21 for several depths in a Eurasian earth structure. This example was calculated for an earthquake with strike 0, dip 80, and rake 15, observed at an azimuth of 45 degrees. The explosion is at the reference depth of 1 km.

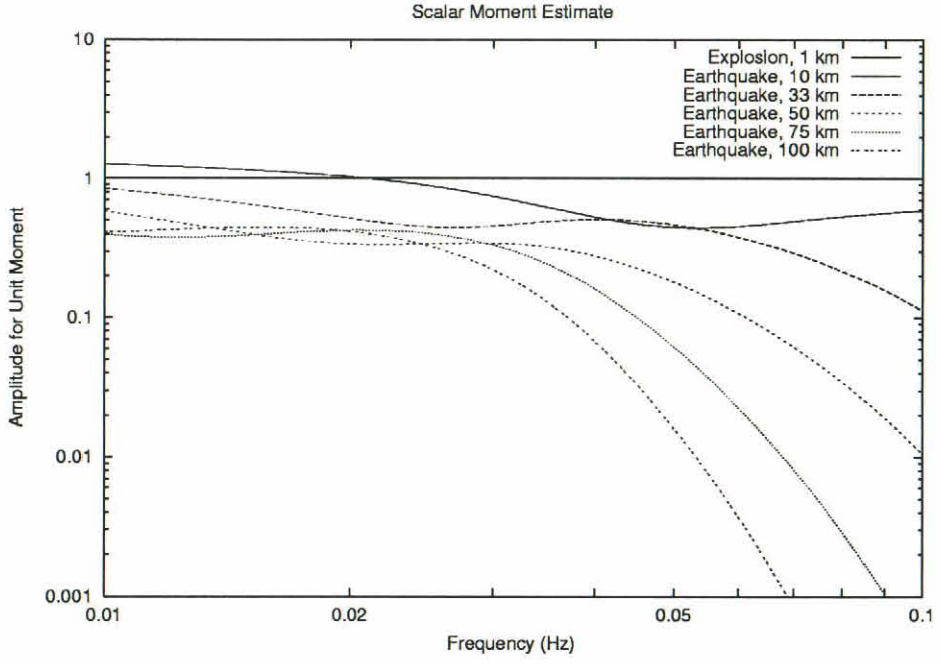

Figure 21. Scalar moment estimate for an explosion and earthquake (Equation 2.5) calculated for several earthquake depths. The spectral amplitude decays more rapidly with increasing frequency for deeper sources.

The surface wave spectral shape/depth discriminant has not been widely used since it was first suggested because of the variability of spectral shape, and dips and peaks that result from path effects and other causes not related to the source, particularly on long, teleseismic paths. Now that we have improved regionalized earth models, however, we can better assess the viability of spectral shape as a depth discriminant.

Figure 22 shows the calculated path corrected spectral magnitudes for all events with known depth for day 2000333 (Julian day 333 in year 2000). Here we have averaged the spectra over a narrow range near each frequency point to smooth out spectral dips, averaged the spectra for all stations observing each event, and divided by the value at 0.01 Hz. The results resemble the calculated values of Figure 21 in some respects. The deepest event at 133 km does have the steepest spectral slope, and the slope generally increases from shallow to deep. However the depth dependent spectral decrease with frequency does not appear to be as strong as predicted in the data. Based on these results, the surface wave spectral shape does not appear to be consistent enough to make a reliable depth discriminant.

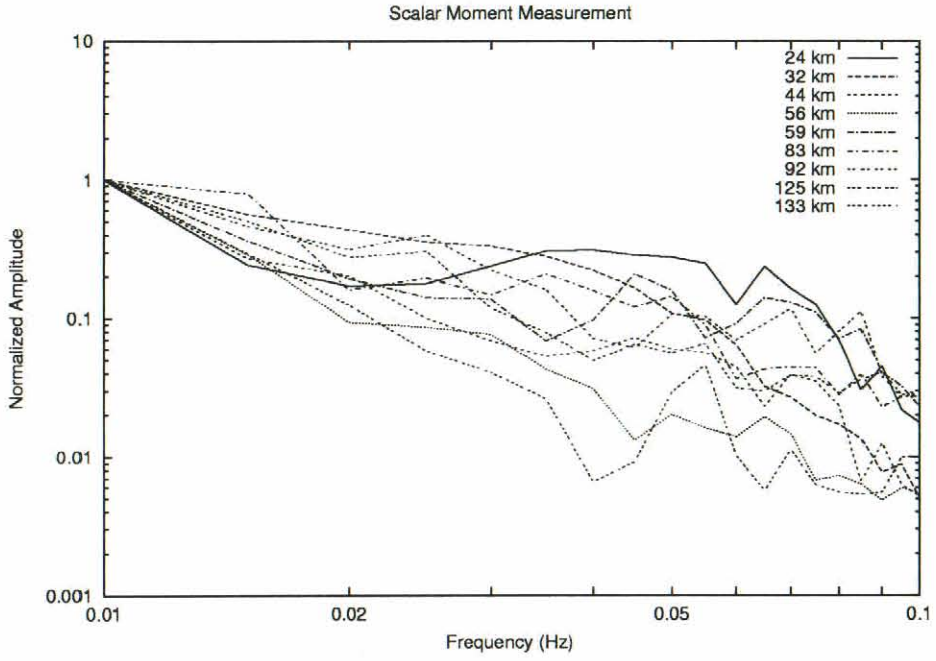

Figure 22. Observed path corrected spectral magnitudes for events with a range of depths for day 2000333.

Section 8
Conclusions and Recommendations

This study has focused on development of improved methods for detection and measurement of surface waves. As part of this effort, we have developed a gradually improving set of global earth models suitable for calculation of phase and group velocity dispersion curves. Over the course of this study, the earth models have evolved from a five degree model based on 90,000 dispersion measurements to a one degree model based on over 500,000 measurements. The inversion procedure allows shallow structure and Moho depth to vary on a one degree grid over approximately 550 distinct crust and upper mantle models. In section 4, we discussed detailed recommendations for improving the results further. We have used phase-velocities derived from these models to form phase-matched filters, and developed an improvement on the surface wave detection algorithm that uses phase-matched filtering followed by narrow-band filtering for detection. We performed a test on one day of data at the PIDC with several dispersion models and found a significant improvement using this technique. We have also tested the use of surface waves for location. Although we cannot confirm improvement as significant as suggested by Yacoub (2000), it does appear that surface waves can add an additional constraint that could significantly improve location, particularly in cases where there are only a few P arrivals and the surface waves are measured on short paths.

Section 9
References

Bassin, C., Laske, G. and Masters, G. (2000), The Current Limits of Resolution for Surface Wave Tomography in North America, EOS Trans AGU, 81, F897.

Berry, M. (1992), Large scale singular value computations, *Int. J. Supercomp. Appl., 6, 13-49.*

Douglas, A., J. A. Hudson and V. K. Kembhavi (1971), "The Relative Excitation of Seismic Surface and Body Waves by Point Sources," *Geophys. J. R. astr. Soc.*, v. 23, pp. 451-460.

Ekstrom, G., A. M. Dziewonski, G. P. Smith, and W. Su (1996), "Elastic and Inelastic Structure Beneath Eurasia," in *Proceedings of the 18th Annual Seismic Research Symposium on Monitoring a Comprehensive Test Ban Treaty*, Phillips Laboratory Report PL-TR-96-2153.

Herrin, E. and T. Goforth (1977), "Phase-Matched Filtering: Application to the Study of Rayleigh Waves," *Bull. Seism. Soc. Am.*, v. 67, pp. 1259-1275.

Kennett, B.L.N. Engdahl, E.R. and Buland, R. (1995), Constraints on seismic velocities in the Earth from travel times, *Geophys J Int*, **122,** 108-124.

Laske G., and G. Masters (1997), A Global Digital Map of Sediment Thickness, *EOS Trans. AGU, 78.*

Laske, G., Masters, G. and Reif C., Crust 2.0 (2001), A new global crustal model at 2*2 degrees, http://mahi.ucsd.edu/Gabi/rem.html.

Levshin, A. L., M. H. Ritzwoller, and S. S. Smith (1996), "Group Velocity Variations Across Eurasia," in *Proceedings of the 18th Annual Seismic Research Symposium on Monitoring A Comprehensive Test Ban Treaty,* Phillips Laboratory Report PL-TR-96-2153.

Marshall, P. D. and P. W. Basham (1972), "Discrimination Between Earthquakes and Underground Nuclear Explosions Employing An Improved Ms scale," *Geophys. J. R. astr. Soc.*, v. 28, pp. 431-458.

Mitchell, B. J., L. Cong and J. Xie, (1996), "Seismic Attenuation Studies in the Middle East and Southern Asia", St. Louis University Scientific Report No. 1, PL-TR-96-2154, ADA317387.

Mooney, W., G. Laske, and G. Masters (1998), "Crust 5.1: A Global Crustal Model at 5x5 Degrees," *Journal of Geophysical Research*, v. 103, no. B1, pp. 727-747.

Müller, R. D., R. R. Roest, J. Royer, L. M. Gahagan, and J. G. Sclater (1997), "Digital isochrons of the world's ocean floor", *J. Geophys. Res.*, 102, 3211-3214.

Nolet, G. (1987), "Seismic Wave Propagation and Seismic Tomography," in *Seismic Tomography with Applications In Global Seismology and Exploration Geophysics*, G. Nolet, ed., D. Reidel Publishing, Dordrecht, Holland.

Rezapour, M. and R. G. Pearce (1998), "Bias in Surface-Wave Magnitude Ms due to Inadequate Distance Corrections," *Bull. Seism. Soc. Am.*, v. 88, pp. 43-61.

Ritzwoller, M. H., A. L. Levshin, L. I. Ratnikova, and D. M. Tremblay (1996), "High Resolution Group Velocity Variations Across Central Asia," in *Proceedings of the 18th Annual Seismic Research Symposium On Monitoring A Comprehensive Test Ban Treaty.*

Ritzwoller, M.H., O.Y Vdovin, and A.L. Levshin (1999), "Surface wave dispersion across Antarctica: A first look", *Antarctic J. U.S.*, in press.

Stevens, J. L. (1986), "Estimation of Scalar Moments From Explosion-Generated Surface Waves," *Bull. Seism. Soc. Am.*, v. 76, pp. 123-151.

Stevens, J. L., Adams, D.A., and Baker, G. E. (2001), "Phase-matched filtering with a one degree dispersion model" Proceedings of the 23rd Annual DOD/DOE Seismic Research Symposium, 1-5 October 2001.

Stevens, Jeffry L., and David A. Adams (1999), "Improved Methods for Regionalized Surface Wave Analysis," Proceedings of the 21st Seismic Research Symposium on Monitoring a Comprehensive Test Ban Treaty, 21-24 September, 1999.

Stevens, J. L., and Adams, D.A. (2000), Improved Surface Wave Detection and Measurement Using Phase-Matched Filtering and Improved Regionalized Models, Proceedings of the 22nd Annual DOD/DOE Seismic Research Symposium, 12-15 September.

Stevens, J. L. and S. M. Day (1985), "The Physical Basis of the mb:Ms and Variable Frequency Magnitude Methods for Earthquake/Explosion Discrimination," *Journal of Geophysical Research*, v. 90, pp. 3009-3020.

Stevens, J. L. and K. L. McLaughlin (1996), "Regionalized Maximum Likelihood Surface Wave Analysis," Maxwell Technologies Technical Report PL-TR-96-2273, SSS-DTR-96-15562, September.

Stevens, J. L., and K. L. McLaughlin (1988), "Analysis of surface waves from the Novaya Zemlya, Mururoa, and Amchitka test sites, and maximum likelihood estimation of scalar moments from earthquakes and explosions," S-CUBED technical report SSS-TR-89-9953, September.

Stevens, J. L. and K. L. McLaughlin (2001), "Optimization of surface wave identification and measurement," *Pure and Applied Geophysics*, v. 158, no. 7, pp 1547-1582.

Tsai, Y.B. and K. Aki (1971), "Amplitude spectra of surface waves from small earthquakes and underground nuclear explosions," *Journal of Geophysical Research, v. 76*, pp. 3940-3952.
Vasco, D. W., L.R. Johnson, and O. Marques (1999), Global Earth structure: inference and assessment, *Geophys. J. Int.,* 137.

Vdovin, O. Y., J. A. Rial, M. H. Ritzwoller, and A. L. Levshin (1999), "Group-velocity tomography of South America and the surrounding oceans", *Geophys. J. Int.*, 136, 324-330.

Yacoub N. (2000), "Maximum Spectral Energy Arrival Time of Rayleigh Waves for Accurate Epicenter Determination and Location Error Reduction", Proceedings of the 22nd Annual DOD/DOE Seismic Research Symposium, 12-15 September 2000.

Yacoub N. (1996), "Maximum Spectral Energy Arrival Time for Epicenter Estimation, Part 1: Rayleigh Waves," *Seismological Research Letters, v. 67*, p. 62.

Appendix A
Data Deliverable

This report is accompanied by a data deliverable that can be obtained on request as directed by the contracting agency. The data deliverable is in the form of a Unix tar file and contains the following:

1. A directory named "str" containing 64800 earth models. The name of each file is constructed from the longitude, colatitude, and base structure name.

2. A directory named "LP" containing regionalized dispersion curves and other quantities derived from the earth models. Files are as follows:

   LP_grid.LR - grid that identifies one earth structure with each one degree cell.
   LP_vel.LR - group velocity.
   LP_pvel.LR - phase velocity.
   LP_S1.LR - surface wave source region amplitude function.
   LP_S2.LR - surface wave receiver region amplitude function.
   LP_ellip.LR - ellipticity.
   LP_gamma.LR - attenuation coefficients.
   The directory also contains the same files with ".o" extension which contain the grid and data file in binary form to improve performance.

3. A file named "str_numbers" listing the structure name and the corresponding structure number used in LP_grid.LR.

4. A directory named "bin" containing programs LPdisp3 and LPdisp3_frq compiled under the Sun Solaris operating system which can be used to calculate the integrated velocity between any two points on the earth.

Definitions of S1 and S2 may be found in Stevens and McLaughlin (2001).

DEPARTMENT OF DEFENSE

DEFENSE TECHNICAL INFORMATION CENTER
8725 JOHN J. KINGMAN ROAD
SUITE 0944
FORT BELVOIR, VA 22060-0944
2 CYS ATTN: DTIC/OCA

DEFENSE THREAT REDUCTION AGENCY
8725 JOHN J. KINGMAN ROAD
MS 6201
FORT BELVOIR, VA 22060-6218
ATTN: D. BARBER

DEPARTMENT OF DEFENSE CONTRACTORS

ITT INDUSTRIES
ITT SYSTEMS CORPORATION
1680 TEXAS STREET, SE
KIRTLAND AFB, NM 87117-5669
2 CYS ATTN: DTRIAC
ATTN: DARE

SCIENCE APPLICATIONS INTERNATIONAL
CORPORATION
10260 CAMPUS DRIVE
SAN DIEGO, CA 92121
ATTN: J. STEVENS